Physics of Fluids

RESEARCH ARTICLE | SEPTEMBER 18 2024

A novel variable-coefficient extended Davey–Stewartson system for internal waves in the presence of background flows

Jun-Chao Sun ; Xiao-Yan Tang ; Yong Chen

Check for updates

Physics of Fluids 36, 097142 (2024)
https://doi.org/10.1063/5.0219224

View Online
Export Citation

21 September 2024 04:25:04

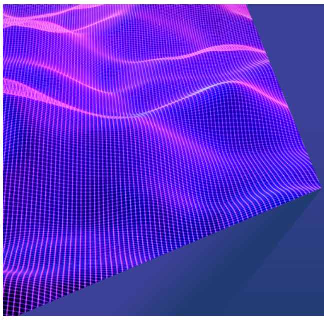

Physics of Fluids
Special Topic:
Flow Engineering with Smart Interfaces
Guest Editors: Xu Chu and Guang Yang
Submit Today!
AIP Publishing

AIP Publishing

Physics of Fluids ARTICLE pubs.aip.org/aip/pof

A novel variable-coefficient extended Davey–Stewartson system for internal waves in the presence of background flows

Cite as: Phys. Fluids **36**, 097142 (2024); doi: 10.1063/5.0219224
Submitted: 16 May 2024 · Accepted: 22 August 2024 ·
Published Online: 18 September 2024

View Online Export Citation CrossMark

Jun-Chao Sun,[1] Xiao-Yan Tang,[1,a)] and Yong Chen[1,2]

AFFILIATIONS

[1]School of Mathematical Sciences, Key Laboratory of Mathematics and Engineering Applications (Ministry of Education) and Shanghai Key Laboratory of PMMP, East China Normal University, Shanghai 200241, China
[2]College of Mathematics and Systems Science, Shandong University of Science and Technology, Qingdao 266590, China

[a)]Author to whom correspondence should be addressed: xytang@sist.ecnu.edu.cn

ABSTRACT

We propose a novel variable-coefficient Davey–Stewartson type system for studying internal wave phenomena in finite-depth stratified fluids with background flows, where the upper- and lower-layer fluids possess distinct velocity potentials, and the variable-coefficient terms are primarily controlled by the background flows. This realizes the first application of variable-coefficient DS-type equations in the field of internal waves. Compared to commonly used internal wave models, this system not only describes multiple types of internal waves, such as internal solitary waves, internal breathers, and internal rogue waves, but also aids in analyzing the impact of background flows on internal waves. We provide the influence of different background flow patterns on the dynamic behavior and spatial position of internal waves, which contribute to a deeper understanding of the mechanisms through which background flows influence internal waves. Furthermore, the system is capable of capturing variations in the velocity potentials of the upper and lower layers. We discover a connection between internal waves under the influence of background flows and velocity potentials. Through the variations in velocity potentials within the flow field, the dynamic behaviors of internal waves can be indirectly inferred, their amplitude positions located, and different types of internal waves distinguished. This result may help address the current shortcomings in satellite detection of internal wave dynamics and internal rogue waves.

Published under an exclusive license by AIP Publishing. https://doi.org/10.1063/5.0219224

21 September 2024 04:25:04

I. INTRODUCTION

Internal waves (IWs) are oscillations within a fluid medium, not on its surface.[1,2] Their existence relies on the stratification of the fluid. Typically, this means density varies with depth. IWs propagate along boundaries where low-density water covers high-density water. Due to the stratified nature of real-world ocean, IWs are ubiquitous in the global ocean.[3,4] The significant vertical displacement and strong horizontal currents induced by them play a crucial role in oceanic ecosystems and energy transfer.[5] Particularly, IWs with larger amplitudes pose potential hazards to ships and offshore drilling platforms.[6] Hence, IWs are of paramount importance for ocean engineering, ecology, and marine resource exploitation.

Since Nansen first discovered the phenomenon of IWs, scholars have conducted extensive observational studies on it.[7] These observations not only reveal the presence of IWs in environments such as lakes and oceans but also discover many types of IWs. From the 1970s to the 1980s, the development of nonlinear internal wave theory significantly advanced the understanding of internal waves. The propositions of equations such as Korteweg–de Vries (KdV), nonlinear Schrödinger (NLS), and Gardner enable us to better describe and comprehend various internal wave phenomena.[8–10] It is found from current oceanic observational data that the IWs exhibit diverse waveforms and complex wave structures. In particular, the propagation of internal solitary waves (ISWs) is more common in small sea areas or nearshore shelf–slope regions.[11,12] Describing and understanding these structurally complex types of IWs necessitates the support of nonlinear theories. Furthermore, the generation and propagation of IWs are influenced by multiple factors. Among them, background flow is one of the primary factors, referring to the dominant flow patterns in oceans or lakes, typically driven by factors such as topography, tides, and large-scale circulation. Early in Benney's original weakly nonlinear description of IWs, background flow was taken into account.[13] Subsequent studies show that variations in background flows significantly affect the amplitude of IWs and may even trigger their breaking and the generation of turbulence.[14,15] Therefore, a thorough investigation of background flows contributes to a better understanding of the generation and propagation of IWs.

Currently, research on different types of IWs primarily utilizes various one-dimensional models. Grimshaw *et al.* studied the propagation of ISWs on slope-shelf topography based on the KdV equation.[16] Bokaeeyan *et al.* found the "bright and dark" solutions of the Gardner equation, which could simulate internal rogue waves (IRWs) in a three-layer fluid.[17] Nakayama and Lamb proposed that internal breathers (IBs) could be well simulated by exact solutions of the mKdV equation.[18] These are excellent works, but two shortcomings remain: first, they primarily rely on one-dimensional models, and different types of IWs require different models; second, the significant factor of background flows is overlooked. Addressing the first shortcoming, we recently proposed a three-coupled Davey–Stewartson (DS) type system.[19] This system leverages the rich exact solution properties of the DS equation to comprehensively describe various types of internal waves (ISWs, IBs, and IRWs), and to reflect their high-dimensional forms. Moreover, considering that the DS equation can describe not only the amplitude but also the velocity potential, this system can be used to investigate the relationship between internal waves and velocity potential. However, we still neglected the role of background flows. In the exploration of IWs, scholars typically separate background flows, assuming they depend only on depth, and mainly investigate their effect on the amplitude.[20] In fact, in the actual marine environment, background flows also vary with time. Therefore, we consider incorporating background flows into variable-coefficient terms and addressing the second limitation with the variable-coefficient DS-type system.[21–23] It is well known that variable-coefficient equations are commonly used in the field of integrable systems to study the dynamics of localized waves.[24–26] Consequently, employing the variable-coefficient system can effectively explore the impact of background flows on the dynamic behavior of internal waves, which has not been fully realized in previous internal wave models. It is worth mentioning that traditional variable-coefficient DS equations (1) are typically used to describe the phenomena in the fields of the ultra-relativistic degenerate dense plasmas or Bose–Einstein condensates[27]

$$
\begin{aligned}
iu_t + P_1(t)u_{xx} + P_2(t)u_{yy} - \left[Q_1(t)|u|^2 + Q_2(t)v\right]u = 0,\\
Rv_{xx} - v_{yy} - S(|u|^2)_{xx} = 0,
\end{aligned}
\tag{1}
$$

where $P_1(t)$ and $P_2(t)$ denote the wave group dispersion; $Q_1(t)$ and $Q_2(t)$ stand for the cubic nonlinear coefficient and nonlocal quadratic nonlinearity, respectively; and R and S are both the constants that represent different physical quantities in different fields. In this paper, we show that the inapplicability of Eq. (1) to IWs in stratified fluids, while also pioneering the extension of variable-coefficient DS-type equations to the field of IWs, thereby establishing a new variable-coefficient system for IWs.

Ocean observation data indicate that at specific observation points, fluctuations exist in parameters such as density, temperature, and velocity inside the ocean, suggesting the possible passage of IWs through these points.[28–30] Compared to traditional internal wave models,[31,32] our proposed variable-coefficient system not only captures various internal wave phenomena but also has the ability to obtain velocity potential information. In previous studies, we have established the existence of a correlation between IWs and velocity potentials.[19] Satellite remote sensing technology is widely used to monitor IWs in the ocean.[33–35] However, the movement speed of IWs is typically fast, and the temporal resolution of satellite remote sensing data may not be sufficient to capture the rapid changes of IWs, limiting the in-depth study of internal wave dynamics. We propose a potential strategy, focusing on utilizing velocity potential information to indirectly infer the presence and dynamics of IWs.

The remaining part of this paper is organized as follows. In Sec. II, we establish a new variable-coefficient system to investigate the effect of background flows on IWs. The physical significance of each parameter is explained, especially the part where background flows is introduced into the variable-coefficient terms. In Sec. III, we introduce a precise solution strategy based on the Hirota bilinear method to obtain the solutions for different types of IWs. The application of the established system in IWs is discussed, and the dynamic behaviors of different types of IWs under the influence of background flows are described in detail. In particular, we emphasize the potential value of velocity potential as an indirect probe for detecting the presence and dynamic behavior of IWs under the influence of background flows in practical applications. Section IV specifically discusses these conclusions, summarizes the main findings, and explores future research directions.

II. DERIVATION OF THE VARIABLE-COEFFICIENT EXTENDED DS SYSTEM

Consider a three-dimensional two-layer fluid system with no viscosity, incompressibility, and no rotation. The velocity potentials of each layer are different. As shown in Fig. 1, let ρ_1 and ρ_2 denote the densities of the upper and lower layers of the fluid, respectively, with depths d_1 and d_2. The depth of the fluid is relatively small compared to the wavelength of the disturbance. The upper and lower layers flow horizontally (in the x direction) with velocities Ψ_1 and Ψ_2, respectively, which are functions solely dependent on time t. The IWs are generated at the interface between the two-layer fluid, and their governing equations can be expressed as follows:

$$
\frac{\partial^2\varphi_1}{\partial x^2} + \frac{\partial^2\varphi_1}{\partial y^2} + \frac{\partial^2\varphi_1}{\partial z^2} = 0, \quad 0 < z < d_1, \tag{2}
$$

$$
\frac{\partial^2\varphi_2}{\partial x^2} + \frac{\partial^2\varphi_2}{\partial y^2} + \frac{\partial^2\varphi_2}{\partial z^2} = 0, \quad -d_2 < z < 0, \tag{3}
$$

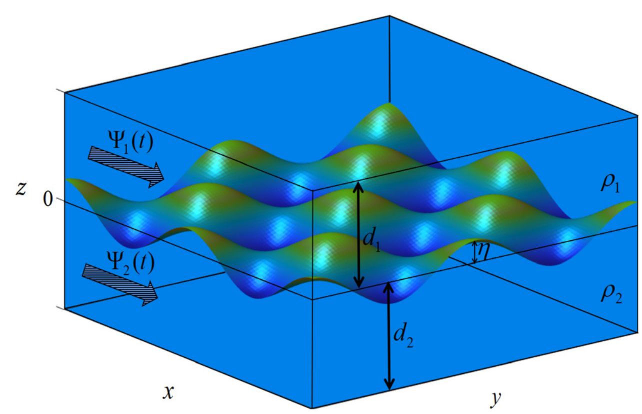

FIG. 1. Schematic view of the flow coordinate system.

21 September 2024 04:25:04

Published under an exclusive license by AIP Publishing

$$\frac{\partial \varphi_1}{\partial z}\Big|_{z=0} = \frac{\partial \eta}{\partial t} + [\Psi_1(t) + U_1]\frac{\partial \eta}{\partial x} + V_1\frac{\partial \eta}{\partial y}, \quad z = \eta(x, y, t), \tag{4}$$

$$\frac{\partial \varphi_2}{\partial z}\Big|_{z=0} = \frac{\partial \eta}{\partial t} + [\Psi_2(t) + U_2]\frac{\partial \eta}{\partial x} + V_2\frac{\partial \eta}{\partial y}, \quad z = \eta(x, y, t), \tag{5}$$

$$p_1 = p_2, \quad z = \eta(x, y, t), \tag{6}$$

$$p_1 = -\rho_1\frac{\partial \varphi_1}{\partial t} - \frac{\rho_1}{2}\{[\Psi_1(t) + U_1]^2 + V_1^2 + W_1^2\} - \rho_1 g\eta, \tag{7}$$

$$p_2 = -\rho_2\frac{\partial \varphi_2}{\partial t} - \frac{\rho_2}{2}\{[\Psi_2(t) + U_2]^2 + V_2^2 + W_2^2\} - \rho_2 g\eta, \tag{8}$$

$$\frac{\partial \varphi_1}{\partial z} = 0, \quad z = d_1, \tag{9}$$

$$\frac{\partial \varphi_2}{\partial z} = 0, \quad z = -d_2, \tag{10}$$

where the velocity potentials of the upper and lower layers are denoted as φ_1 and φ_2, respectively, while $\eta(x, y, t)$ represents the amplitude of the waves at the interface. V_i and W_i are the components of fluid velocity in the y and z directions, respectively, and due to the presence of background flows, the component of fluid velocity in the x direction is $\Psi_i(t) + U_i$, where $i = 1$ represents the upper layer and $i = 2$ represents the lower layer. Because of the assumption of small wave amplitudes, the values of quantities at $z = \eta$ are still replaced by $z = 0$. At the interface, pressure should be continuous; thus, $p_1 = p_2$ represents the dynamic boundary condition. Equations (9) and (10), respectively, characterize the constraints imposed on the fluid by rigid boundaries at the top and bottom.

Introduce appropriate reference quantities to construct dimensionless variables: $\hat{x} = \frac{x}{\lambda}$, $\hat{y} = \frac{y}{\lambda}$, $\hat{z} = \frac{x}{h}$, $\hat{t} = \frac{c}{\lambda}t$, $\hat{\eta} = \frac{\eta}{\vartheta}$, $\hat{\varphi_1} = \frac{h}{\vartheta\lambda c}\varphi_1$, $\hat{\varphi_2} = \frac{h}{\vartheta\lambda c}\varphi_2$, where λ, ϑ, and h represent typical wavelength, typical amplitude, and typical water depth, respectively, and $c = \sqrt{gh}$ denotes the typical horizontal velocity. Using these dimensionless quantities, Eqs. (2)–(10) can be reformulated as follows:

$$\delta\left(\frac{\partial^2 \varphi_1}{\partial x^2} + \frac{\partial^2 \varphi_1}{\partial y^2}\right) + \frac{\partial^2 \varphi_1}{\partial z^2} = 0, \quad 0 < z < \frac{d_1}{h}, \tag{11}$$

$$\delta\left(\frac{\partial^2 \varphi_2}{\partial x^2} + \frac{\partial^2 \varphi_2}{\partial y^2}\right) + \frac{\partial^2 \varphi_2}{\partial z^2} = 0, \quad -\frac{d_2}{h} < z < 0, \tag{12}$$

$$\delta\left(\frac{\partial \eta}{\partial t} + \varepsilon\frac{\partial \varphi_1}{\partial x}\frac{\partial \eta}{\partial x} + \varepsilon\frac{\partial \varphi_1}{\partial y}\frac{\partial \eta}{\partial y}\right) - \frac{\partial \varphi_1}{\partial z} = 0, \quad z = \varepsilon\eta(x, y, t), \tag{13}$$

$$\delta\left(\frac{\partial \eta}{\partial t} + \varepsilon\frac{\partial \varphi_2}{\partial x}\frac{\partial \eta}{\partial x} + \varepsilon\frac{\partial \varphi_2}{\partial y}\frac{\partial \eta}{\partial y}\right) - \frac{\partial \varphi_2}{\partial z} = 0, \quad z = \varepsilon\eta(x, y, t), \tag{14}$$

$$\begin{aligned}\rho_1\frac{\partial \varphi_1}{\partial t} + \rho_1\eta + \frac{\rho_1}{2}\left[\varepsilon\left(\frac{\partial \varphi_1}{\partial x}\right)^2 + \varepsilon\left(\frac{\partial \varphi_1}{\partial y}\right)^2\right] + \frac{\rho_1\varepsilon}{2\delta}\left(\frac{\partial \varphi_1}{\partial z}\right)^2 \\ = \rho_2\frac{\partial \varphi_2}{\partial t} + \rho_2\eta + \frac{\rho_2}{2}\left[\varepsilon\left(\frac{\partial \varphi_2}{\partial x}\right)^2 + \varepsilon\left(\frac{\partial \varphi_2}{\partial y}\right)^2\right] + \frac{\rho_2\varepsilon}{2\delta}\left(\frac{\partial \varphi_2}{\partial z}\right)^2, \\ z = \varepsilon\eta(x, y, t),\end{aligned} \tag{15}$$

$$\frac{\partial \varphi_1}{\partial z} = 0, \quad z = d_1, \tag{16}$$

$$\frac{\partial \varphi_2}{\partial z} = 0, \quad z = -d_2. \tag{17}$$

The above equations are often more concise and general, capable of reflecting the fundamental characteristics of internal wave phenomenon. Here, $\varepsilon = \frac{\vartheta}{h}$ is the nonlinear (amplitude) parameter and $\delta = \frac{h^2}{\lambda^2}$ is the dispersion (long wavelength) parameter.

The velocity potentials consist of two parts: the velocity potential of the background flow and the velocity potential of the wave motion. To further simplify Eqs. (11)–(17), we perform a multi-scale expansion on the wave velocity potentials under the long wave condition, given by

$$\varphi_1 = \Psi_1(t)x + \varphi_{10} + \delta\varphi_{11} + \delta^2\varphi_{12} + \delta^3\varphi_{13} + \cdots, \tag{18}$$

$$\varphi_2 = \Psi_2(t)x + \varphi_{20} + \delta\varphi_{21} + \delta^2\varphi_{22} + \delta^3\varphi_{23} + \cdots. \tag{19}$$

Under the assumption of long waves, we have $\delta \ll 1$.

Substituting Eqs. (18) and (19) into Eqs. (11), (12), (16), and (17), and then collecting terms of the same order of δ, we obtain

$$\delta^0: \ \varphi_{10} = \varphi_{10}(x, y, t), \quad \varphi_{20} = \varphi_{20}(x, y, t), \tag{20}$$

$$\begin{aligned}\delta^1: \ \varphi_{11} &= -\frac{\left(z - \frac{d_1}{h}\right)^2}{2}\left(\frac{\partial u_1}{\partial x} + \frac{\partial v_1}{\partial y}\right), \\ \varphi_{21} &= -\frac{\left(z + \frac{d_2}{h}\right)^2}{2}\left(\frac{\partial u_2}{\partial x} + \frac{\partial v_2}{\partial y}\right),\end{aligned} \tag{21}$$

$$\delta^2: \begin{aligned}\varphi_{12} &= \frac{\left(z - \frac{d_1}{h}\right)^4}{24}\left(\frac{\partial}{\partial x}(\nabla^2 u_1) + \frac{\partial}{\partial y}(\nabla^2 v_1)\right), \\ \varphi_{22} &= \frac{\left(z + \frac{d_2}{h}\right)^4}{24}\left(\frac{\partial}{\partial x}(\nabla^2 u_2) + \frac{\partial}{\partial y}(\nabla^2 v_2)\right),\end{aligned} \tag{22}$$

where $\frac{\partial\varphi_{10}}{\partial x} = u_1$, $\frac{\partial\varphi_{10}}{\partial y} = v_1$, $\frac{\partial\varphi_{20}}{\partial x} = u_2$ and $\frac{\partial\varphi_{20}}{\partial y} = v_2$.

According to equations (18)–(22), we can simplify system (11)–(17) as follows:

$$\begin{aligned}\frac{1}{\delta}\left[\frac{\partial \eta}{\partial t} - \frac{d_1}{h}\left(\frac{\partial u_1}{\partial x} + \frac{\partial v_1}{\partial y}\right)\right] + U_r\left[\frac{\partial(u_1\eta)}{\partial x} + \frac{\partial(v_1\eta)}{\partial y} + \Psi_1(t)\frac{\partial \eta}{\partial x}\right] \\ -\frac{1}{6}\left(\frac{-d_1}{h}\right)^3\left[\frac{\partial}{\partial x}(\nabla^2 u_1) + \frac{\partial}{\partial y}(\nabla^2 v_1)\right] = 0,\end{aligned} \tag{23}$$

$$\begin{aligned}\frac{1}{\delta}\left[\frac{\partial \eta}{\partial t} + \frac{d_2}{h}\left(\frac{\partial u_2}{\partial x} + \frac{\partial v_2}{\partial y}\right)\right] + U_r\left[\frac{\partial(u_2\eta)}{\partial x} + \frac{\partial(v_2\eta)}{\partial y} + \Psi_2(t)\frac{\partial \eta}{\partial x}\right] \\ -\frac{1}{6}\left(\frac{d_2}{h}\right)^3\left[\frac{\partial}{\partial x}(\nabla^2 u_2) + \frac{\partial}{\partial y}(\nabla^2 v_2)\right] = 0,\end{aligned} \tag{24}$$

$$\begin{aligned}\frac{\rho_1}{\delta}\left[\frac{\partial u_1}{\partial t} + \frac{\partial \eta}{\partial x} + \frac{d\Psi_1(t)}{dt}\right] + \rho_1 U_r\left\{[u_1 + \Psi_1(t)]\frac{\partial u_1}{\partial x} + v_1\frac{\partial u_1}{\partial y}\right\} \\ -\frac{\rho_1}{2}\left(\frac{-d_1}{h}\right)^2\frac{\partial}{\partial t}(\nabla^2 u_1) \\ = \frac{\rho_2}{\delta}\left(\frac{\partial u_2}{\partial t} + \frac{\partial \eta}{\partial x} + \frac{d\Psi_2(t)}{dt}\right) + \rho_2 U_r\left\{[u_2 + \Psi_2(t)]\frac{\partial u_2}{\partial x} + v_2\frac{\partial u_2}{\partial y}\right\} \\ -\frac{\rho_2}{2}\left(\frac{d_2}{h}\right)^2\frac{\partial}{\partial t}(\nabla^2 u_2),\end{aligned} \tag{25}$$

21 September 2024 04:25:04

Published under an exclusive license by AIP Publishing

$$\frac{\rho_1}{\delta}\left(\frac{\partial v_1}{\partial t}+\frac{\partial \eta}{\partial y}\right)+\rho_1 U_r\left\{[u_1+\Psi_1(t)]\frac{\partial v_1}{\partial x}+v_1\frac{\partial v_1}{\partial y}\right\}$$
$$-\frac{\rho_1}{2}\left(\frac{-d_1}{h}\right)^2\frac{\partial}{\partial t}(\nabla^2 v_1)$$
$$=\frac{\rho_2}{\delta}\left(\frac{\partial v_2}{\partial t}+\frac{\partial \eta}{\partial y}\right)+\rho_2 U_r\left\{[u_2+\Psi_2(t)]\frac{\partial v_2}{\partial x}+v_2\frac{\partial v_2}{\partial y}\right\}$$
$$-\frac{\rho_2}{2}\left(\frac{d_2}{h}\right)^2\frac{\partial}{\partial t}(\nabla^2 v_2), \tag{26}$$

where $U_r=\frac{\varepsilon}{\delta}$ is the Ursell parameter.

However, Eqs. (23)–(26) still form a set of complex nonlinear equations. In order to obtain precise solutions describing IWs and velocity potentials, we adopt the method of multiple scales.[36] First, we introduce new variables

$$\xi=\varepsilon(x-C_g t),\quad \theta=\varepsilon y,\quad \tau=\varepsilon^2 t, \tag{27}$$

where C_g is the group velocity and ε is a small parameter.

To obtain approximate equations for studying the behavior of Eqs. (23)–(26), we represent the dependent variables in the form of the sum of the main variation and modification terms

$$u_j=\sum_{n=1}^{\infty}\varepsilon^n\sum_{m=-n}^{n}E^m u_{jn}^{(m)}(\xi,\theta,\tau),\quad v_j=\sum_{n=2}^{\infty}\varepsilon^n\sum_{m=-n}^{n}E^m v_{jn}^{(m)}(\xi,\theta,\tau),$$
$$\eta=\sum_{n=1}^{\infty}\varepsilon^n\sum_{m=-n}^{n}E^m\eta_n^{(m)}(\xi,\theta,\tau),\quad \Psi_j=\sum_{n=0}^{\infty}\varepsilon^n\Psi_{jn}(\tau), \tag{28}$$

where $E=e^{i(kx-\omega t)}$, $\eta_n^{(-m)}=\eta_n^{*(m)}$, $u_{jn}^{(-m)}=u_{jn}^{*(m)}$, and $v_{jn}^{(-m)}=v_{jn}^{*(m)}$, with the star denoting the complex conjugate.

Next, we concentrate on the main variation terms determined by low powers of ε. Substituting Eqs. (27) and (28) into Eqs. (23)–(26), terms of the same order in $\varepsilon^n E^m$ are collected. At the order of ε^1E^1, we obtain

$$u_{11}^{(1)}=\frac{6h^3[\Psi_{10}(\tau)kU_r\delta-\omega]}{kd_1(d_1^2k^2\delta+6h^2)}\eta_1^{(1)},$$
$$u_{21}^{(1)}=\frac{6h^3[\Psi_{20}(\tau)kU_r\delta-\omega]}{kd_2(d_2^2k^2\delta+6h^2)}\eta_1^{(1)}. \tag{29}$$

The coefficients for $\varepsilon^2E^0,\varepsilon^2E^1$, and ε^2E^2 give rise to the following relation:

$$\eta_1^{(0)}=0,\quad u_{11}^{(0)}=0,\quad u_{21}^{(0)}=0,\quad \frac{d\Psi_{20}(\tau)}{d\tau}=\frac{\rho_1}{\rho_2}\left[\frac{d\Psi_{10}(\tau)}{d\tau}\right], \tag{30}$$

$$u_{12}^{(1)}=iS_1(\tau)\frac{\partial\eta_1^{(1)}}{\partial\xi}+S_2(\tau)\eta_1^{(1)},\quad u_{22}^{(1)}=iF_1(\tau)\frac{\partial\eta_1^{(1)}}{\partial\xi}+F_2(\tau)\eta_1^{(1)},$$
$$\eta_2^{(1)}=iW_1(\tau)\frac{\partial\eta_1^{(1)}}{\partial\xi}+W_2(\tau)\eta_1^{(1)}, \tag{31}$$

$$v_{12}^{(1)}=iJ_1(\tau)\frac{\partial\eta_1^{(1)}}{\partial\theta},\quad v_{22}^{(1)}=iJ_2(\tau)\frac{\partial\eta_1^{(1)}}{\partial\theta}, \tag{32}$$

$$u_{12}^{(2)}=P_1(\tau)\left(\eta_1^{(1)}\right)^2,\quad u_{22}^{(2)}=M_1(\tau)\left(\eta_1^{(1)}\right)^2,\quad \eta_2^{(2)}=G_1(\tau)\left(\eta_1^{(1)}\right)^2, \tag{33}$$

$$v_{12}^{(2)}=0,\quad v_{22}^{(2)}=0, \tag{34}$$

where $S_1(\tau)$, $S_2(\tau)$, $F_1(\tau)$, $F_2(\tau)$, $W_1(\tau)$, $W_2(\tau)$, $J_1(\tau)$, $J_2(\tau)$, $P_1(\tau)$, $M_1(\tau)$, and $G_1(\tau)$ are given in Appendix.

According to Eqs. (29)–(34), the following system is finally obtained:

$$a_1(\tau)\frac{\partial^2\phi_1}{\partial\xi^2}+a_2(\tau)\frac{\partial^2\phi_1}{\partial\theta^2}+a_3(\tau)\frac{\partial\phi_2}{\partial\xi^2}-a_4(\tau)\frac{\partial|\eta_1^{(1)}|^2}{\partial\xi}=0, \tag{35}$$

$$b_1(\tau)\frac{\partial^2\phi_2}{\partial\xi^2}+b_2(\tau)\frac{\partial^2\phi_2}{\partial\theta^2}+b_3(\tau)\frac{\partial\phi_1}{\partial\xi^2}-b_4(\tau)\frac{\partial|\eta_1^{(1)}|^2}{\partial\xi}=0, \tag{36}$$

$$ic_1(\tau)\frac{\partial\eta_1^{(1)}}{\partial\tau}+c_2(\tau)\frac{\partial^2\eta_1^{(1)}}{\partial\xi^2}+c_3(\tau)\frac{\partial^2\eta_1^{(1)}}{\partial\theta^2}+c_4(\tau)|\eta_1^{(1)}|^2\eta_1^{(1)}$$
$$+c_5(\tau)\eta_1^{(1)}\frac{\partial\phi_1}{\partial\xi}+c_6(\tau)\eta_1^{(1)}\frac{\partial\phi_2}{\partial\xi}+ic_7(\tau)\frac{\partial\eta_1^{(1)}}{\partial\xi}$$
$$+[ic_8(\tau)+c_9(\tau)]\eta_1^{(1)}=0. \tag{37}$$

Here, $\eta_1^{(1)}$ represents the complex amplitude variable, and the real functions ϕ_1 and ϕ_2 can be regarded as velocity potential variables. Additionally, $\frac{\partial\phi_1}{\partial\xi}=u_{12}^{(0)}$, $\frac{\partial\phi_1}{\partial\theta}=v_{12}^{(0)}$, $\frac{\partial\phi_2}{\partial\xi}=u_{22}^{(0)}$ and $\frac{\partial\phi_2}{\partial\theta}=v_{22}^{(0)}$, $\frac{d\Psi_{21}(\tau)}{d\tau}=\frac{\rho_1}{\rho_2}[\frac{d\Psi_{11}(\tau)}{d\tau}]$, $\frac{d\Psi_{22}(\tau)}{d\tau}=\frac{\rho_1}{\rho_2}[\frac{d\Psi_{12}(\tau)}{d\tau}]$. $a_i(\tau)$, $b_i(\tau)$ and $c_j(\tau)$ $(i=1,\ldots,4$ and $j=1,\ldots,9)$ are variable coefficients only dependent on τ, and their expressions are provided in the Appendix.

Compared with the equations commonly used in previous studies of IWs, the system consisting of (35)–(37) not only accounts for the IWs in stratified fluids with high-dimensional effects but also provides information on the velocity potentials of the upper and lower layers, which are not achievable with previous models of IWs.[16–18] In contrast to the classical variable-coefficient DS equation (1), Eqs. (35)–(37) introduce additional terms such as $\frac{\partial\eta_1^{(1)}}{\partial\xi}$ and $\eta_1^{(1)}$, and incorporate more variable coefficients such as a_i and b_i $(i=1,2)$. This may lead to novel outcomes. When $\phi_1=\phi_2$ and $a_i=b_i$ $(i=1,2)$, Eqs. (35)–(37) reduce to the classical variable-coefficient DS equation with additional terms

$$[a_1(\tau)+a_3(\tau)]\frac{\partial^2\phi_1}{\partial\xi^2}+a_2(\tau)\frac{\partial^2\phi_1}{\partial\theta^2}+a_4(\tau)\frac{\partial|\eta_1^{(1)}|^2}{\partial\xi}=0,$$
$$ic_1(\tau)\frac{\partial\eta_1^{(1)}}{\partial\tau}+c_2(\tau)\frac{\partial^2\eta_1^{(1)}}{\partial\xi^2}+c_3(\tau)\frac{\partial^2\eta_1^{(1)}}{\partial\theta^2}+c_4(\tau)|\eta_1^{(1)}|^2\eta_1^{(1)}$$
$$+[c_5(\tau)+c_6(\tau)]\eta_1^{(1)}\frac{\partial\phi_1}{\partial\xi}+ic_7(\tau)\frac{\partial\eta_1^{(1)}}{\partial\xi}$$
$$+[ic_8(\tau)+c_9(\tau)]\eta_1^{(1)}=0. \tag{38}$$

It is noteworthy that negative density or equal densities in upper and lower layers appear in this transformation process, indicating the inability of the classical variable-coefficient DS equation to directly describe the phenomenon of IWs in stratified fluids. However, further mathematical investigations into Eq. (38) are warranted for future exploration.

In summary, we have constructed, for the first time, a novel variable-coefficient system to describe the velocity potentials and IWs in density-stable stratified fluids. Since it has partial resemblance to Eq. (1), we refer to it as the variable-coefficient extended DS (VCEDS) equation.

21 September 2024 04:25:04

Published under an exclusive license by AIP Publishing

The coefficients of the VCEDS equation are highly complex, involving multiple physical quantities such as background flow, density, depth, dispersion parameters, and Ursell parameters, resulting in coefficients with high degrees of freedom. In the remaining part of this paper, we will focus on the time-dependent background flows, while other physical quantities constitute arbitrary constants. In other words, these coefficients can be viewed as polynomials of the background flows, while the specific physical analysis of these coefficients is left for future work.

III. INTERNAL WAVES

To capture the internal wave phenomenon that can be characterized by the system (35)–(37) and investigate the influence of background flows on IWs, we make the following transformations to the amplitude, upper-, and lower-layer velocity potentials:[22,27]

$$\eta_1^{(1)} = \frac{G}{F}, \quad \phi_1 = \alpha(\tau)(\ln F)_\xi + A, \quad \phi_2 = \beta(\tau)(\ln F)_\xi + B, \tag{39}$$

where F is a real function and G is a complex function, $\alpha(\tau)$ and $\beta(\tau)$ are parameter variables that depend solely on τ, and A and B are constants. Note that $\alpha(\tau) \neq \beta(\tau)$ and $A \neq B$, so that $\phi_1 \neq \phi_2$.

Substituting Eq. (39) into the system (35)–(37), we obtain the bilinear form

$$\begin{cases} \left\{[a_1(\tau)\alpha(\tau) + a_3(\tau)\beta(\tau)]D_\xi^2 + a_2(\tau)\alpha(\tau)D_\theta^2 - R(\tau)\right\}F\cdot F \\ \quad + 2a_4(\tau)G\cdot G^* = 0, \\ \left\{[b_1(\tau)\beta(\tau) + b_3(\tau)\alpha(\tau)]D_\xi^2 + b_2(\tau)\beta(\tau)D_\theta^2 - K(\tau)\right\}F\cdot F \\ \quad + 2b_4(\tau)G\cdot G^* = 0, \\ \left[\mathrm{i}c_1(\tau)D_\tau + c_2(\tau)D_\xi^2 + c_3(\tau)D_\theta^2 + \mathrm{i}c_7(\tau)D_\xi + \mathrm{i}c_8(\tau) + c_9(\tau) - C(\tau)\right] \\ \quad \times G\cdot F = 0, \\ \left\{\left[c_2(\tau) - \frac{1}{2}c_5(\tau)\alpha(\tau) - \frac{1}{2}c_6(\tau)\beta(\tau)\right]D_\xi^2 + c_3(\tau)D_\theta^2 - C(\tau)\right\}F\cdot F \\ \quad - c_4(\tau)G\cdot G^* = 0, \end{cases} \tag{40}$$

where R, K, and C are parameter variables that depend solely on τ, while D_ξ, D_θ, and D_τ are the bilinear differential operators defined as follows:[37]

$$D_\xi^m D_\theta^l D_\tau^k(F, G) = \left(\frac{\partial}{\partial \xi} - \frac{\partial}{\partial \xi'}\right)^m \left(\frac{\partial}{\partial \theta} - \frac{\partial}{\partial \theta'}\right)^l \left(\frac{\partial}{\partial \tau} - \frac{\partial}{\partial \tau'}\right)^k FG\big|_{\xi'=\xi,\theta'=\theta,\tau'=\tau}. \tag{41}$$

A. Internal solitary waves

For the purpose of exploring the applicability of Eqs. (35)–(37) in describing ISWs and researching the effect of variable coefficients controlled by background flows on their propagation, we assume

$$G = n e^{\mathrm{i}a(\tau)}\left[1 + n_1 e^{p\xi + q\theta + \Omega(\tau) + \mathrm{i}\gamma}\right], \quad F = 1 + n_1 e^{p\xi + q\theta + \Omega(\tau)}, \tag{42}$$

where n, n_1, p, q, and γ are constants, while $a(\tau)$ and $\Omega(\tau)$ will be determined subsequently and can represent interventions and adjustments of the background flows.

Substituting Eq. (42) into Eq. (40), we obtain the solution for ISWs

$$\eta_1^{(1)} = \frac{n e^{\mathrm{i}a(\tau)}\left[1 + n_1 e^{p\xi + q\theta + \Omega(\tau) + \mathrm{i}\gamma}\right]}{1 + n_1 e^{p\xi + q\theta + \Omega(\tau)}}, \tag{43}$$

where

$$a(\tau) = \int \frac{c_4(\tau)n^2 + c_9(\tau)}{c_1(\tau)} d\tau, \quad \Omega(\tau) = \int \frac{-c_7(\tau)p}{c_1(\tau)} d\tau. \tag{44}$$

In comparison with models commonly used to describe IWs, Eqs. (35)–(37) can also provide solutions for the velocity potentials

$$\phi_1 = \alpha(\tau)\cdot \frac{p n_1 e^{p\xi + q\theta + \Omega(\tau)}}{1 + n_1 e^{p\xi + q\theta + \Omega(\tau)}} + A, \tag{45}$$

$$\phi_2 = \beta(\tau)\cdot \frac{p n_1 e^{p\xi + q\theta + \Omega(\tau)}}{1 + n_1 e^{p\xi + q\theta + \Omega(\tau)}} + B, \tag{46}$$

where $\alpha(\tau)$ and $\beta(\tau)$ are given by

$$\begin{aligned} \alpha(\tau) = \{&2c_2(\tau)n^2[\cos(\gamma)a_3(\tau)c_3(\tau)b_5(\tau) + \cos(\gamma)a_5(\tau)c_2(\tau)b_2(\tau) \\ &- \cos(\gamma)a_5(\tau)c_3(\tau)b_1(\tau) - a_3(\tau)c_3(\tau)b_5(\tau) - a_5(\tau)c_2(\tau)b_2(\tau) \\ &+ a_5(\tau)c_3(\tau)b_1(\tau)]\}/\{q^2[a_3(\tau)c_3(\tau)^2b_3(\tau) \\ &+ a_1(\tau)c_2(\tau)c_3(\tau)b_2(\tau) - a_1(\tau)c_3(\tau)^2b_1(\tau) \\ &- a_2(\tau)c_2(\tau)^2b_2(\tau) + a_2(\tau)c_2(\tau)c_3(\tau)b_1(\tau)]\}, \end{aligned} \tag{47}$$

$$\begin{aligned} \beta(\tau) = -\{&2c_2(\tau)n^2[\cos(\gamma)a_1(\tau)c_3(\tau)b_5(\tau) - \cos(\gamma)a_2(\tau)c_2(\tau)b_5(\tau) \\ &+ a_5(\tau)c_3(\tau)b_3(\tau) - \cos(\gamma)a_5(\tau)c_3(\tau)b_3(\tau) \\ &- a_1(\tau)c_3(\tau)b_5(\tau) + a_2(\tau)c_2(\tau)b_5(\tau)]\}/\{q^2[a_3(\tau)c_3(\tau)^2b_3(\tau) \\ &+ a_1(\tau)c_2(\tau)c_3(\tau)b_2(\tau) - a_1(\tau)c_3(\tau)^2b_1(\tau) \\ &- a_2(\tau)c_2(\tau)^2b_2(\tau) + a_2(\tau)c_2(\tau)c_3(\tau)b_1(\tau)]\}. \end{aligned} \tag{48}$$

It is worth noting that to achieve the above results, we must satisfy the condition $c_8 = 0$. Fortunately, this condition is feasible, just making sure that Ψ_{10} and Ψ_{20} are both constants or $d_1 = d_2$. Therefore, the generation and propagation of ISWs can be divided into two cases. The first case is that the main variation terms of the background flows in the upper and lower layers are both constants, and the second is that the depths of the upper and lower layers are equal.

The first case is illustrated in Fig. 2. The secondary variations of the background flows are set to be periodic functions, linear functions, and constants, respectively, resulting in three types of dynamic behaviors of ISWs. The most common type of ISWs [see Fig. 2(c)] is obtained, when all the variations of the background flows are constant, a situation that usually corresponds to regions without significant flow variations. They propagate linearly at a uniform speed, because no background flow velocity variations affect the wave propagation characteristics. At this time, the VCEDS system degenerates into a constant-coefficient form. However, when the background flows increase linearly over time, ISWs no longer propagate linearly but instead bend [see Fig. 2(b)]. On the other hand, when the background flows vary periodically, ISWs also exhibit periodic dynamic behavior [see Fig. 2(a)]. This periodic variation can be considered a modulation of the ISWs, causing ISWs to display periodic behavior corresponding

21 September 2024 04:25:04

Published under an exclusive license by AIP Publishing

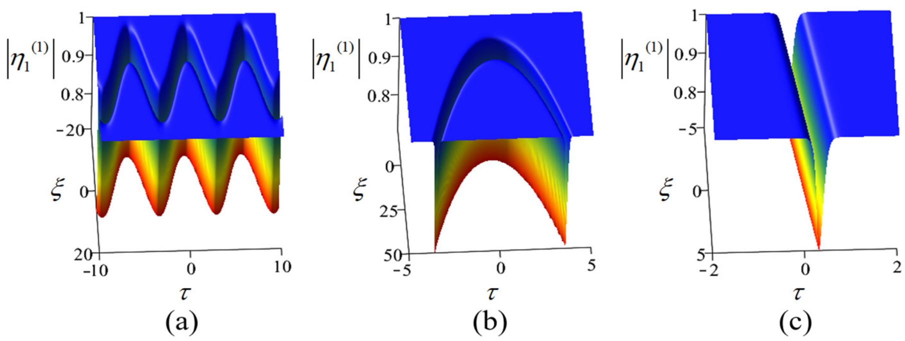

FIG. 2. The dynamic behaviors of the internal solitary waves with $\Psi_{10} = 2$. (a) $\Psi_{11} = \Psi_{12} = \sin(\tau)$, (b) $\Psi_{11} = \Psi_{12} = \tau$, and (c) $\Psi_{11} = \Psi_{12} = 2$.

to the changes in the background flows. The above results reveal that the background flows have a significant influence on the dynamic behaviors of ISWs. The response of the ISWs to the variation of the background flows also demonstrates the adaptability and variability of IWs under different flow field conditions. In addition, we obtain the variations of the upper and lower velocity potentials during the propagation of the ISWs (see Fig. 3), a capability not provided by general models. Together with Fig. 2, it can be roughly observed that the velocity potentials change drastically in the region where the amplitudes fluctuate. Changes in velocity potentials can expose key dynamical characteristics during the propagation of IWs because they determine the velocity distribution and reflect fluid particle motion. The relation between ISWs and velocity potentials is discussed in detail in the subsequent analysis.

The second case is illustrated in Fig. 4. The components of the background flows are set as periodic functions, linear functions, and their combination forms, resulting in four types of internal solitary wave dynamics. Periodic functions result in ISWs exhibiting periodic dynamic behavior [see Fig. 4(a)], while linear functions cause the propagation of ISWs to bend [see Fig. 4(b)], similar to the first case. However, the combination forms result in completely irregular dynamic behaviors [see Figs. 4(c) and 4(d)]. The combination of such periodic and linear variations creates a complex flow pattern that makes the behaviors of ISWs more unpredictable. This suggests that in ocean environments, complex variations in background flows may pose a challenge to the detection and prediction of IWs, and thus, there is a need to rely on more suitable models to address this complexity. By comparing Figs. 4(a) and 4(d), it is evident that different primary variations in the background flows lead to distinct dynamic behaviors of ISWs. Similarly, comparing Figs. 4(a) and 4(c) shows that different secondary variations in the background flows also result in varying dynamic behaviors of ISWs. Hence, it can be concluded that both primary and secondary variations in the background flows can significantly affect the dynamic behavior of ISWs. Figure 5 illustrates the corresponding variations in velocity potentials.

As an advantage of high-dimensional models, we are able to conduct research from the perspective of space (ξ, θ). As shown in Fig. 6, at $\tau = 0$, the spatial positions of ISWs vary under different background

21 September 2024 04:25:04

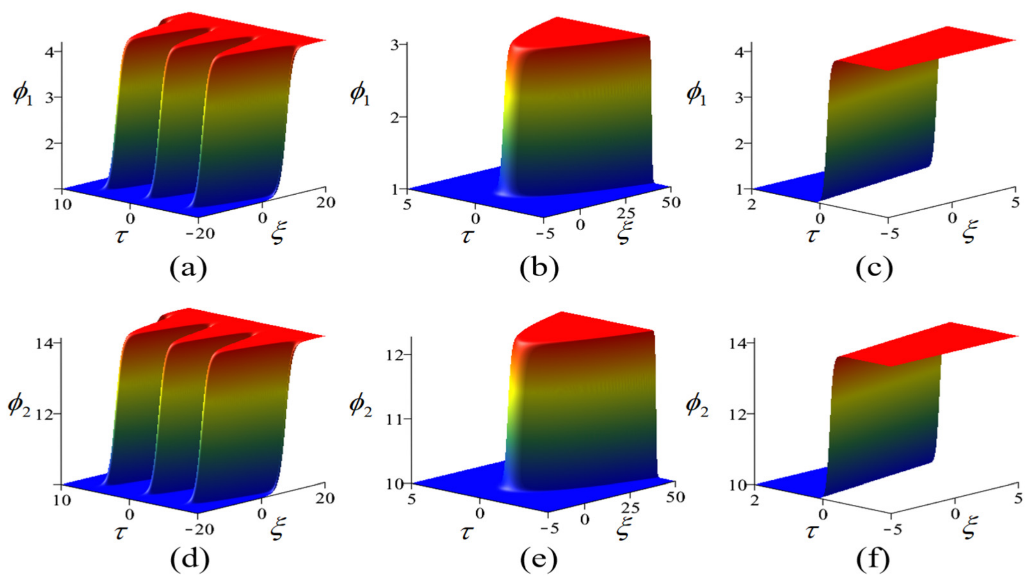

FIG. 3. The upper-layer velocity potential ϕ_1 and the lower-layer velocity potential ϕ_2 of the internal solitary waves with $\Psi_{10} = 2$. (a) $\Psi_{11} = \Psi_{12} = \sin(\tau)$, (b) $\Psi_{11} = \Psi_{12} = \tau$, and (c) $\Psi_{11} = \Psi_{12} = 2$. For (d), (e), and (f), the background flow parameters are the same as those in (a), (b), and (c), respectively.

Published under an exclusive license by AIP Publishing

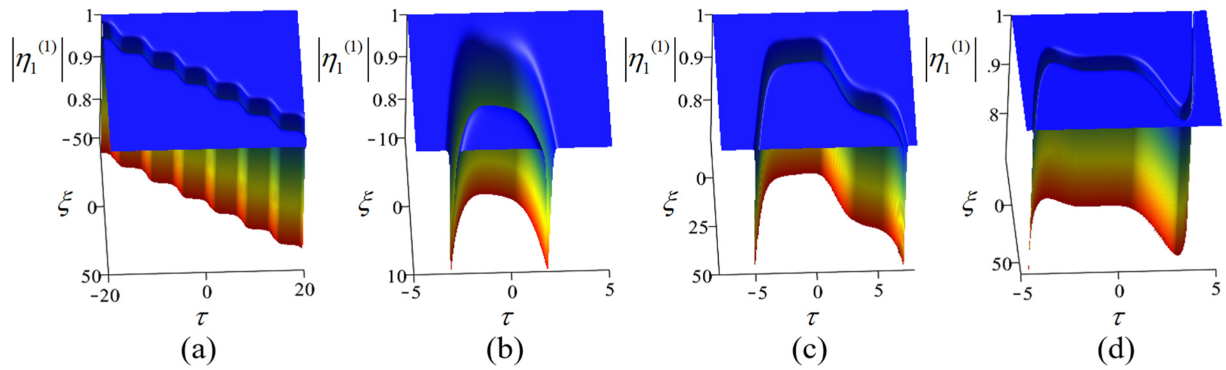

FIG. 4. The dynamic behaviors of the internal solitary waves with $d_1 = d_2$. (a) $\Psi_{10} = \Psi_{11} = \Psi_{12} = \sin(\tau)$, (b) $\Psi_{10} = \Psi_{11} = \Psi_{12} = \tau$, (c) $\Psi_{10} = \sin(\tau)$, $\Psi_{11} = \Psi_{12} = \tau$, and (d) $\Psi_{10} = \tau$, $\Psi_{11} = \Psi_{12} = \sin(\tau)$.

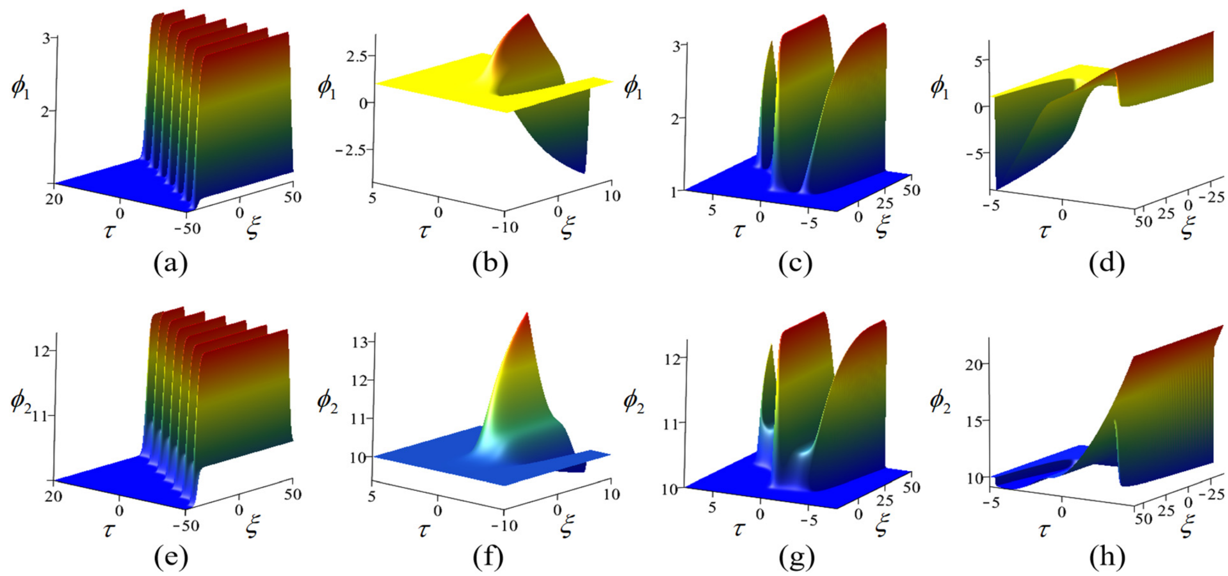

FIG. 5. The upper-layer velocity potential ϕ_1 and the lower-layer velocity potential ϕ_2 of the internal solitary waves with $d_1 = d_2$. (a) $\Psi_{10} = \Psi_{11} = \Psi_{12} = \sin(\tau)$, (b) $\Psi_{10} = \Psi_{11} = \Psi_{12} = \tau$, (c) $\Psi_{10} = \sin(\tau)$, $\Psi_{11} = \Psi_{12} = \tau$, and (d) $\Psi_{10} = \tau$, $\Psi_{11} = \Psi_{12} = \sin(\tau)$. For (e), (f), (g), and (h), the background flow parameters are the same as those in (a), (b), (c), and (d), respectively.

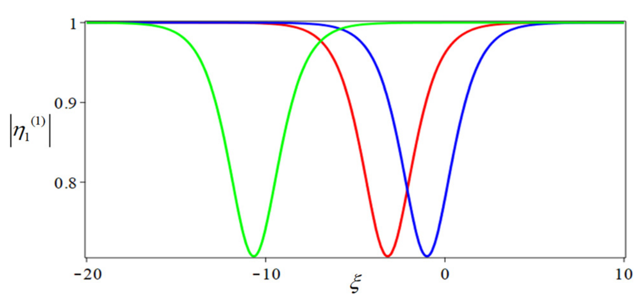

FIG. 6. The internal solitary waves at $\tau = 0$. Color in red: $\Psi_{10} = \Psi_{11} = \Psi_{12} = \sin(\tau)$, in blue: $\Psi_{10} = \Psi_{11} = \Psi_{12} = \tau$, and in green: $\Psi_{10} = 2$, $\Psi_{11} = \Psi_{12} = \sin(\tau)$.

flow patterns. Specifically, the two types of ISWs under periodic background flows are located closer to each other, whereas they are farther away from ISWs under the linear background flow. In addition, the time-dependent background flows do not affect the amplitude and shape of ISWs, which is different from depth-dependent background flows. This implies that the position of the observed ISWs at a certain time may vary with the background flows, while other fundamental properties remain stable. In the 3D plots, we show the spatial characteristics of the ISWs at different moments, using only one background flow pattern as an example. As shown in Fig. 7, the ISWs exhibit the shape of linear solitons propagating with constant amplitude over time. In addition, it is observed that the velocity potentials vary substantially at locations where ISWs appear at different moments, whereas the velocity potentials remain unchanged at locations where

21 September 2024 04:25:04

Published under an exclusive license by AIP Publishing

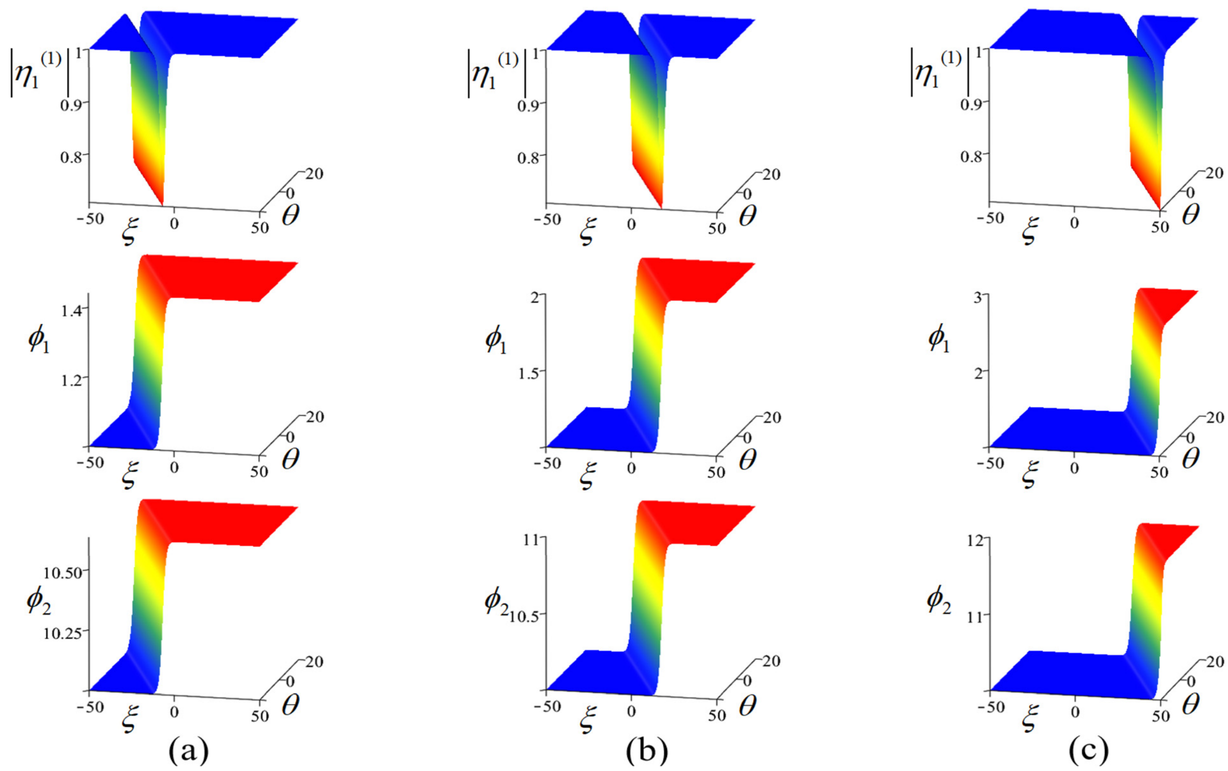

FIG. 7. Evolution of an internal solitary wave and velocity potentials in the (ξ, θ)-plane at time (a) $\tau = -15$, (b) $\tau = 0$, and (c) $\tau = 15$, respectively.

no ISWs appear. The appearance and propagation of ISWs cause significant local changes in the velocity potentials, further supporting the close relation between velocity potentials and ISWs.

By observing the density plots of ISWs and velocity potentials under different background flows in Figs. 8 and 9, it appears that the propagation trajectory of ISWs can perfectly envelope the range of velocity potential variations. To verify this, we superimpose the density plots of ISWs and velocity potentials to illustrate more clearly the degree of coincidence between them (see Fig. 10). It is well known that satellites are the primary tools for detecting ISWs in the ocean, but they can only provide snapshots of a certain moment (as described in Fig. 7), making it difficult to accurately reflect the dynamic behaviors of ISWs. However, real-time monitoring of flow velocities within the marine fluid is relatively easy to achieve. Therefore, we can use the velocity potential field to infer the propagation of ISWs. Furthermore, through Fig. 11, we observe that the locations where the amplitude of ISWs is generated correspond to positions with significant changes in velocity potentials, typically oscillating rapidly between local minima and maxima. Otherwise, the velocity potentials change slowly or remain unchanged. To clearly illustrate this correspondence, we adjust the ratio of A to B from 1 to 10 (in reality the ratio is closer to 1, but the curves will overlap) and mark the positions of maximum amplitude with dashed lines in the figure. Hereafter, we can indirectly infer the propagation of ISWs based on the velocity potential field and determine the spatiotemporal locations of their amplitude occurrence. Note that we obtain the same results from a spatial (ξ, θ) perspective analysis, so it is not further elaborated here.

B. Internal breathers

In this subsection, we investigate IBs by Eqs. (35)–(37) through assuming

$$\begin{aligned} G &= n e^{\mathrm{i}a(\tau)}\{1 + e^{\mathrm{i}[px+qy+\Omega(\tau)]+\gamma_1+\mathrm{i}\gamma_2} \\ &\quad + e^{-\mathrm{i}[px+qy+\Omega(\tau)]+\gamma_1+\mathrm{i}\gamma_2} + n_1 e^{2\gamma_1+2\mathrm{i}\gamma_2}\}, \\ F &= 1 + e^{\mathrm{i}[px+qy+\Omega(\tau)]+\gamma_1} + e^{-\mathrm{i}[px+qy+\Omega(\tau)]+\gamma_1} + n_1 e^{2\gamma_1}, \end{aligned} \tag{49}$$

where n, n_1, p, q, γ_1, and γ_2 are constants, while $a(\tau)$ and $\Omega(\tau)$ are functions solely dependent on τ.

Substituting Eq. (49) into Eqs.(40), we obtain the solution for IBs

$$\eta_1^{(1)} = \frac{n e^{\mathrm{i}a(\tau)}\{1 + e^{\mathrm{i}[px+qy+\Omega(\tau)]+\gamma_1+\mathrm{i}\gamma_2} + e^{-\mathrm{i}[px+qy+\Omega(\tau)]+\gamma_1+\mathrm{i}\gamma_2} + n_1 e^{2\gamma_1+2\mathrm{i}\gamma_2}\}}{1 + e^{\mathrm{i}[px+qy+\Omega(\tau)]+\gamma_1} + e^{-\mathrm{i}[px+qy+\Omega(\tau)]+\gamma_1} + n_1 e^{2\gamma_1}}, \tag{50}$$

where

$$\begin{aligned} a(\tau) &= \int \frac{c_4(\tau)n^2 + c_9(\tau)}{c_1(\tau)}\mathrm{d}\tau, \quad \Omega(\tau) = -\int \frac{c_7(\tau)p}{c_1(\tau)}\mathrm{d}\tau, \\ n_1 &= \frac{4\cos(\gamma_2) - 4}{\cos(2\gamma_2) - 1}. \end{aligned} \tag{51}$$

Published under an exclusive license by AIP Publishing

21 September 2024 04:25:04

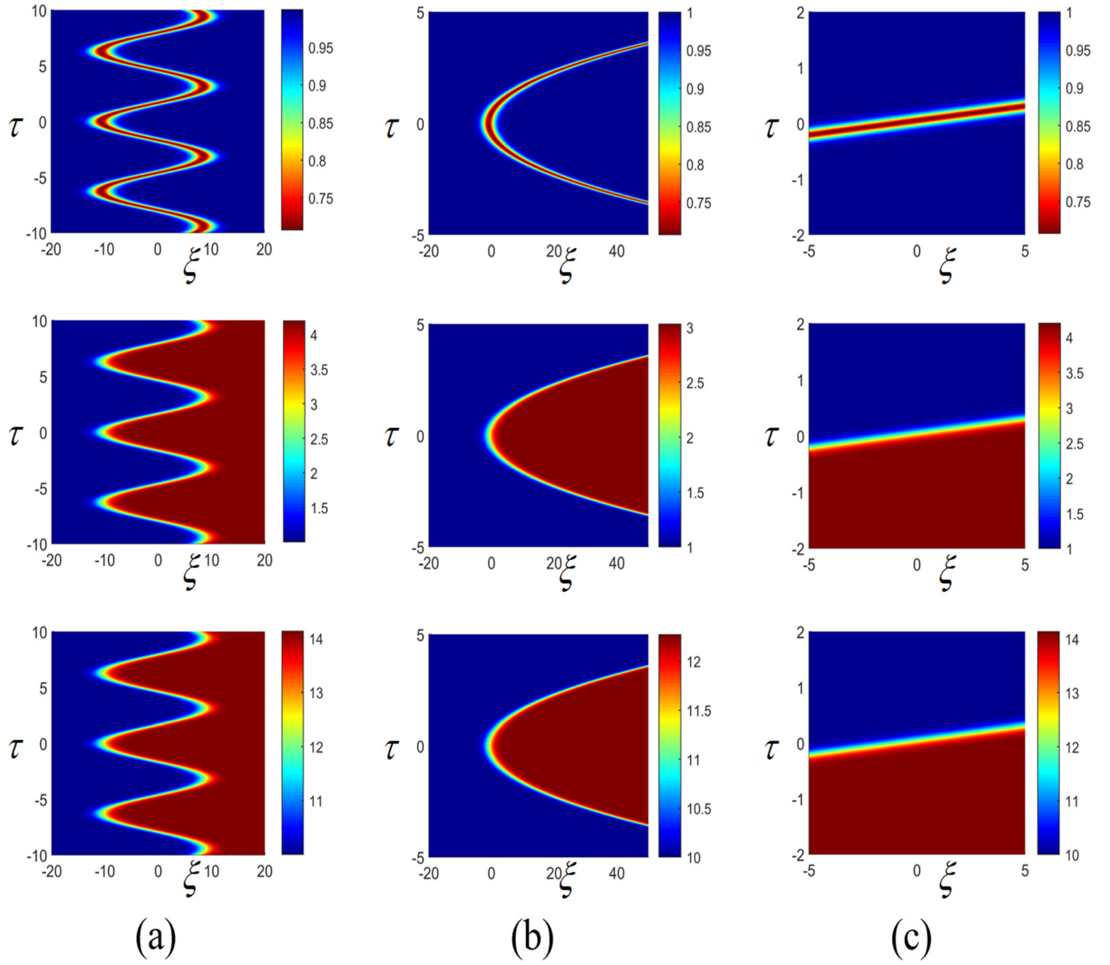

FIG. 8. The density plots of the internal solitary waves and the velocity potentials with $\Psi_{10} = 2$. (a) $\Psi_{11} = \Psi_{12} = \sin(\tau)$, (b) $\Psi_{11} = \Psi_{12} = \tau$, and (c) $\Psi_{11} = \Psi_{12} = 2$.

The solutions for the upper and lower velocity potentials are given as follows:

$$\phi_1 = \alpha(\tau)\cdot\frac{ipe^{i[px+qy+\Omega(\tau)]+\gamma_1} - ipe^{-i[px+qy+\Omega(\tau)]+\gamma_1}}{1+e^{i[px+qy+\Omega(\tau)]+\gamma_1}+e^{-i[px+qy+\Omega(\tau)]+\gamma_1}+\dfrac{4\cos(\Phi)-4}{\cos(2\Phi)-1}e^{2\gamma_1}} + A, \tag{52}$$

$$\phi_2 = \beta(\tau)\cdot\frac{ipe^{i[px+qy+\Omega(\tau)]+\gamma_1} - ipe^{-i[px+qy+\Omega(\tau)]+\gamma_1}}{1+e^{i[px+qy+\Omega(\tau)]+\gamma_1}+e^{-i[px+qy+\Omega(\tau)]+\gamma_1}+\dfrac{4\cos(\Phi)-4}{\cos(2\Phi)-1}e^{2\gamma_1}} + B, \tag{53}$$

where

$$\begin{aligned}\alpha(\tau) = \{&2n^2[\cos(\gamma_2)p^2a_3(\tau)b_5(\tau) - \cos(\gamma_2)p^2a_5(\tau)b_1(\tau)\\ &-\cos(\gamma_2)q^2a_5(\tau)b_2(\tau) - p^2a_3(\tau)b_5(\tau) + q^2a_5(\tau)b_2(\tau)\\ &+p^2a_5(\tau)b_1(\tau)]\}/[p^4a_3(\tau)b_3(\tau) - p^4a_1(\tau)b_1(\tau)\\ &-p^2q^2a_1(\tau)b_2(\tau) - p^2q^2a_2(\tau)b_1(\tau) - q^4a_2(\tau)b_2(\tau)],\end{aligned} \tag{54}$$

$$\begin{aligned}\beta(\tau) = -\{&2n^2[\cos(\gamma_2)p^2a_1(\tau)b_5(\tau) - \cos(\gamma_2)p^2a_5(\tau)b_3(\tau)\\ &+\cos(\gamma_2)q^2a_2(\tau)b_5(\tau) - p^2a_1(\tau)b_5(\tau) - q^2a_2(\tau)b_5(\tau)\\ &+p^2a_5(\tau)b_3(\tau)]\}/[p^4a_3(\tau)b_3(\tau) - p^4a_1(\tau)b_1(\tau)\\ &-p^2q^2a_1(\tau)b_2(\tau) - p^2q^2a_2(\tau)b_1(\tau) - q^4a_2(\tau)b_2(\tau)].\end{aligned} \tag{55}$$

The condition for obtaining the IBs is also $c_8 = 0$. Thus, the IBs described by Eqs. (35)–(37) also fall into two cases: one, where the main variation terms are constants; the other, where the upper and lower depths are equal. When both Ψ_{10} and Ψ_{20} are constants, we set the secondary variations to be periodic functions, linear functions, and constants, respectively, resulting in three types of internal breather dynamics (see Fig. 12). In the case where all the variation terms are constants, conventional IBs are obtained [see Fig. 12(c)], exhibiting periodicity in time and space, with no change in amplitude during propagation. The oscillations within each period are similar to conventional ISWs. In the case of linear functions [see Fig. 12(b)], the propagation process of IBs becomes curved. In the case of periodic functions [see Fig. 12(a)], IBs exhibit a periodically curved propagation process. This result is consistent with the influence of background flows on the

Published under an exclusive license by AIP Publishing
21 September 2024 04:25:04

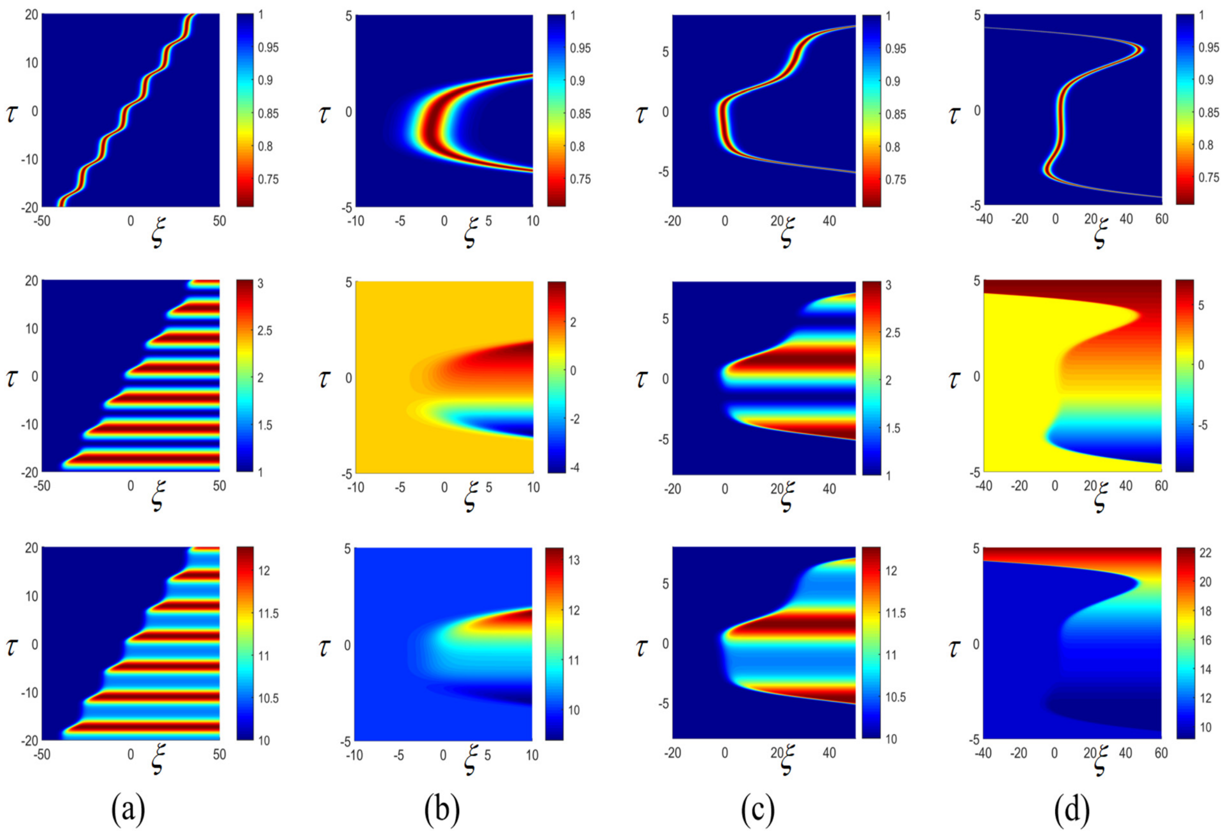

FIG. 9. The density plots of the internal solitary waves and the velocity potentials with $d_1 = d_2$. (a) $\Psi_{10} = \Psi_{11} = \Psi_{12} = \sin(\tau)$, (b) $\Psi_{10} = \Psi_{11} = \Psi_{12} = \tau$, (c) $\Psi_{10} = \sin(\tau)$, $\Psi_{11} = \Psi_{12} = \tau$, and (d) $\Psi_{10} = \tau$, $\Psi_{11} = \Psi_{12} = \sin(\tau)$.

21 September 2024 04:25:04

dynamics of ISWs and shows that changes in background flows can alter the temporal periodicity of IBs. Additionally, variations in the velocity potentials during the propagation of IBs are displayed (see Fig. 13), where the velocity potentials exhibit periodic characteristics similar to those of IBs.

When $d_1 = d_2$, we also consider cases when the variation terms are periodic functions, linear functions, and their combination, resulting in four types of internal breather dynamics (see Fig. 14). The dynamics in Figs. 14(a) and 14(b) are similar to those in Figs. 12(a) and 12(b), caused by the fact that the background flows vary in a similar way over time. The combined forms of background flows also generate complex internal breather dynamics [see Figs. 14(c) and 14(d)], which were rarely reported in previous studies. In the case, we can observe that both the primary and minor variation terms have a significant impact on the IBs, and it is noted that under the same background flows, the dynamic behaviors of IBs within one cycle is similar to that of ISWs, indicating a certain consistency in the influence of background flows on IBs and ISWs. Figure 15 presents the corresponding variations in velocity potentials. It is worth mentioning that when the background flows are constant, ISWs and IBs we obtain are consistent with IWs described by the constant-coefficient DS-type system.[19] These waves can also be regarded as high-dimensional forms of solutions obtained from common low-dimensional internal wave models such as the KdV and mKdV equations.[16,18] In this scenario, the background flows have no significant impact on the dynamics of IWs. However, when the background flows vary with time, the propagation characteristics of IWs are affected, exhibiting various dynamic behaviors. These behaviors reveal the complex diversity of internal wave motions.

Similar to the situation of ISWs, the background flows have no effect on the amplitude of IBs (see Fig. 16). Although the background flows shift the position of IBs, they continue to exhibit spatial periodicity. Figure 17 shows the spatial morphology of IBs at different time, accompanied by images of the velocity potentials in the upper and lower layers. It is evident that the IBs maintain a highly consistent periodicity characteristic with their velocity potentials. Next, by comparing Figs. 18 and 19, we find that the corresponding velocity potentials of IBs exhibits similar density structures. To verify this, the density maps of IBs and velocity potentials are superimposed (see Fig. 20) to clearly demonstrate the good agreement between them. This implies that we can also use the velocity potential field to infer the propagation of IBs. From Figs. 21(c), 21(d), and 21(g), it can be seen that IBs cause the amplitude of IBs to appear periodically, and correspondingly, the velocity potentials also exhibit periodic dramatic changes. Figures 21(a), 21(b), 21(e), and 21(f) show that in regions where no amplitude appears for long durations, the changes in velocity potentials are

Published under an exclusive license by AIP Publishing

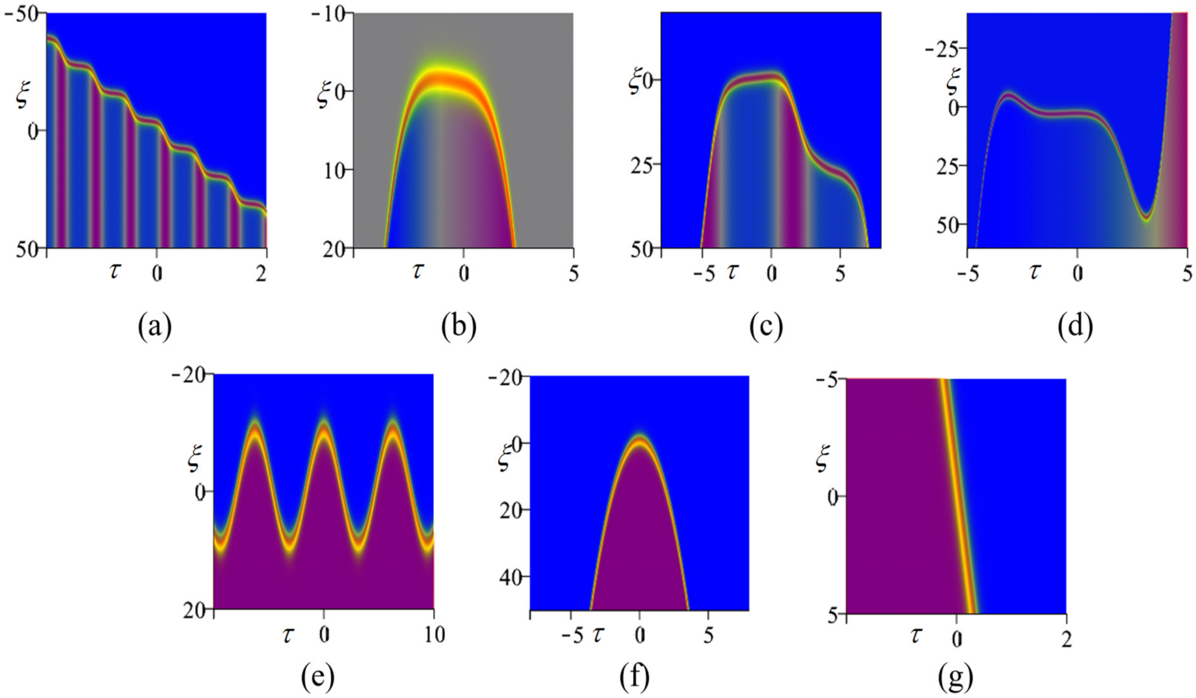

FIG. 10. The velocity potential indirectly infers the dynamic behaviors of internal solitary waves. (a) $\Psi_{10} = 2$, $\Psi_{11} = \Psi_{12} = \sin(\tau)$, (b) $\Psi_{10} = 2$, $\Psi_{11} = \Psi_{12} = \tau$, (c) $\Psi_{10} = \Psi_{11} = \Psi_{12} = 2$, (d) $\Psi_{10} = \Psi_{11} = \Psi_{12} = \sin(\tau)$, (e) $\Psi_{10} = \Psi_{11} = \Psi_{12} = \tau$, (f) $\Psi_{10} = \sin(\tau)$, $\Psi_{11} = \Psi_{12} = \tau$, and (g) $\Psi_{10} = \tau$, $\Psi_{11} = \Psi_{12} = \sin(\tau)$.

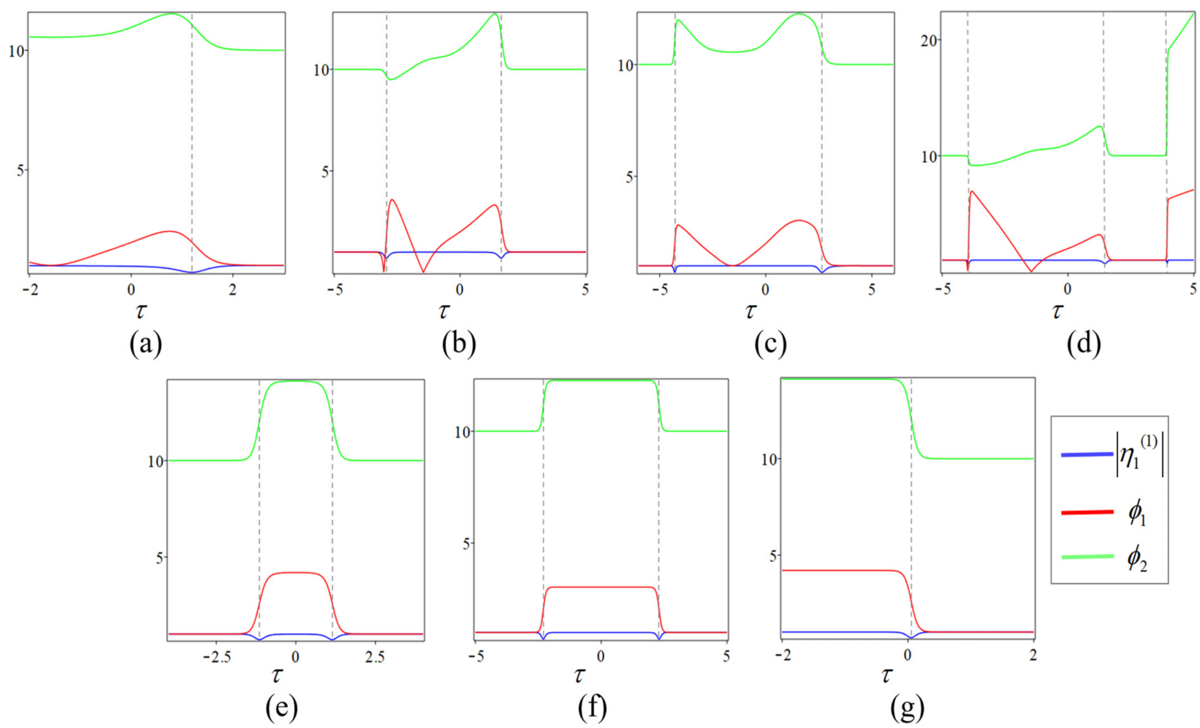

FIG. 11. The velocity potential indirectly infers the appearance of internal solitary waves. (a) $\Psi_{10} = 2$, $\Psi_{11} = \Psi_{12} = \sin(\tau)$, (b) $\Psi_{10} = 2$, $\Psi_{11} = \Psi_{12} = \tau$, (c) $\Psi_{10} = \Psi_{11} = \Psi_{12} = 2$, (d) $\Psi_{10} = \Psi_{11} = \Psi_{12} = \sin(\tau)$, (e) $\Psi_{10} = \Psi_{11} = \Psi_{12} = \tau$, (f) $\Psi_{10} = \sin(\tau)$, $\Psi_{11} = \Psi_{12} = \tau$, and (g) $\Psi_{10} = \tau$, $\Psi_{11} = \Psi_{12} = \sin(\tau)$.

21 September 2024 04:25:04

Published under an exclusive license by AIP Publishing

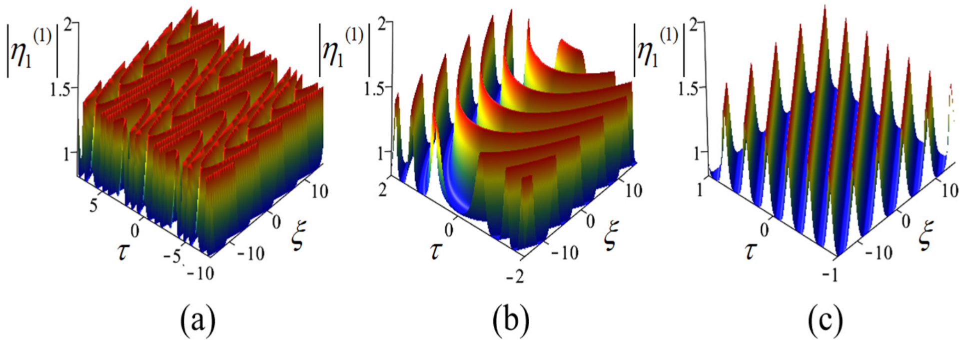

FIG. 12. The dynamic behaviors of the internal breathers with $\Psi_{10} = 2$. (a) $\Psi_{11} = \Psi_{12} = \sin(\tau)$, (b) $\Psi_{11} = \Psi_{12} = \tau$, and (c) $\Psi_{11} = \Psi_{12} = 2$.

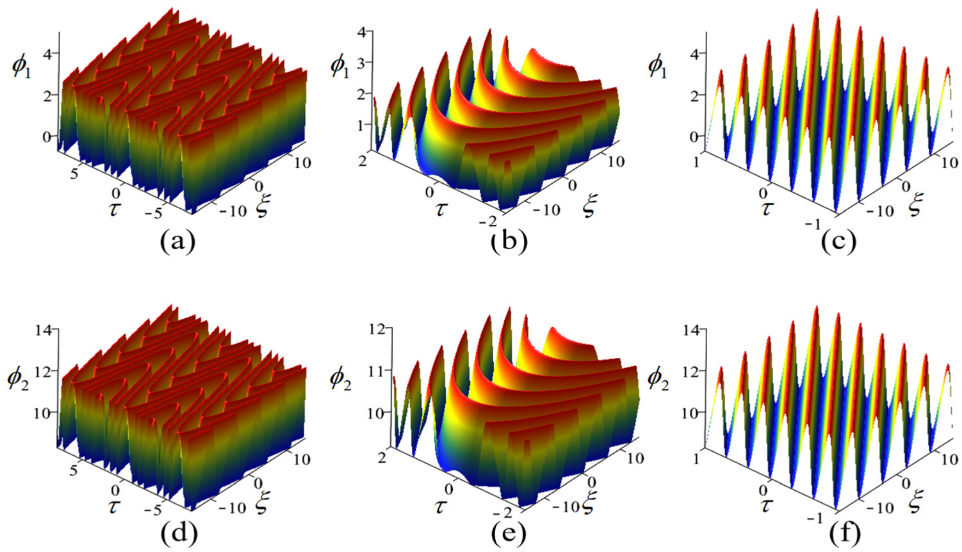

FIG. 13. The upper-layer velocity potential ϕ_1 and the lower-layer velocity potential ϕ_2 of the internal breathers with $\Psi_{10} = 2$. (a) $\Psi_{11} = \Psi_{12} = \sin(\tau)$, (b) $\Psi_{11} = \Psi_{12} = \tau$, and (c) $\Psi_{11} = \Psi_{12} = 2$. For (d), (e), and (f), the background flow parameters are the same as those in (a), (b), and (c), respectively.

21 September 2024 04:25:04

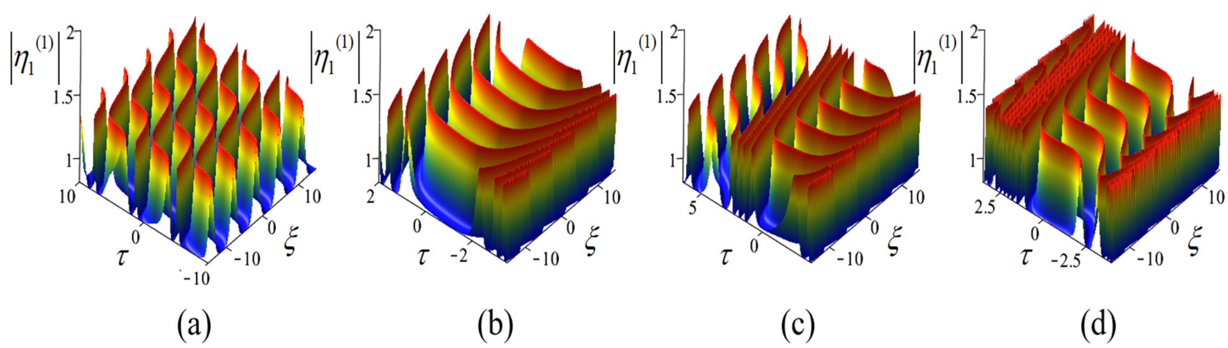

FIG. 14. The dynamic behaviors of the internal breathers with $d_1 = d_2$. (a) $\Psi_{10} = \Psi_{11} = \Psi_{12} = \sin(\tau)$, (b) $\Psi_{10} = \Psi_{11} = \Psi_{12} = \tau$, (c) $\Psi_{10} = \sin(\tau)$, $\Psi_{11} = \Psi_{12} = \tau$, and (d) $\Psi_{10} = \tau$, $\Psi_{11} = \Psi_{12} = \sin(\tau)$.

relatively slow. Once the amplitude appears, the velocity potentials change rapidly. Dashed lines signify the position of maximum amplitude to clearly illustrate this correspondence. Notably, the IBs significantly lose their temporal periodicity in Figs. 21(a), 21(b), 21(e), and 21(f), showing that the background flows disrupt the periodicity of the IBs. The above results indicate that we can also indirectly infer the characteristics of IBs based on the velocity potential field, and further distinguish whether the types of waves generated in the fluid are breathers or solitary waves based on the different characteristics of the velocity potentials.

Published under an exclusive license by AIP Publishing

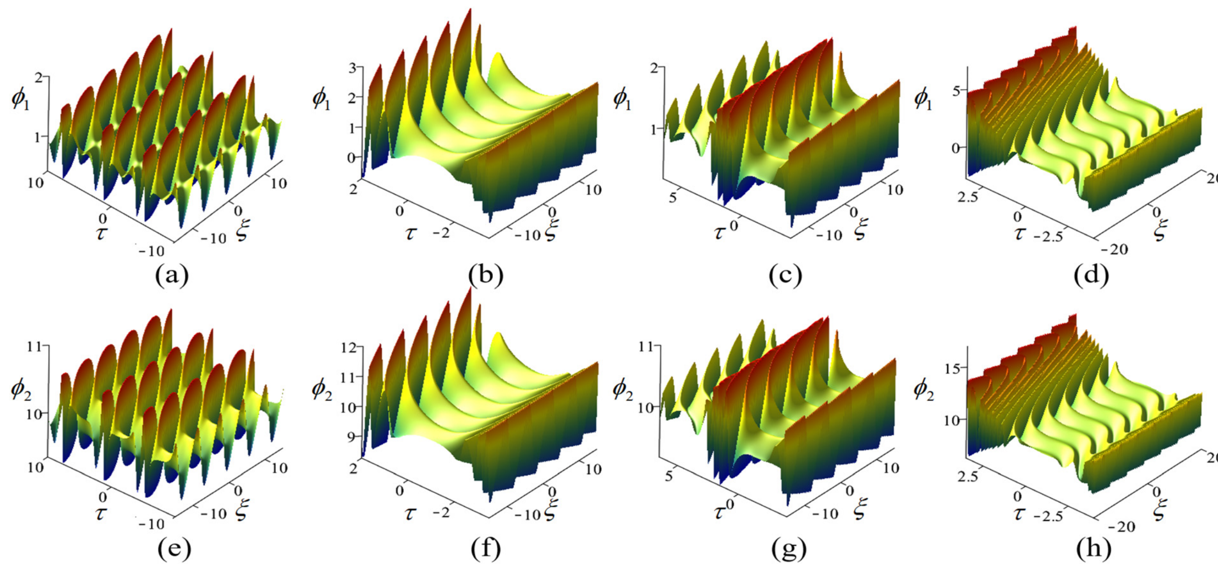

FIG. 15. The upper-layer velocity potential ϕ_1 and the lower-layer velocity potential ϕ_2 of the internal breathers with $d_1 = d_2$. (a) $\Psi_{10} = \Psi_{11} = \Psi_{12} = \sin(\tau)$, (b) $\Psi_{10} = \Psi_{11} = \Psi_{12} = \tau$, (c) $\Psi_{10} = \sin(\tau)$, $\Psi_{11} = \Psi_{12} = \tau$, and (d) $\Psi_{10} = \tau$, $\Psi_{11} = \Psi_{12} = \sin(\tau)$. For (e), (f), (g), and (h), the background flow parameters are the same as those in (a), (b), (c), and (d), respectively.

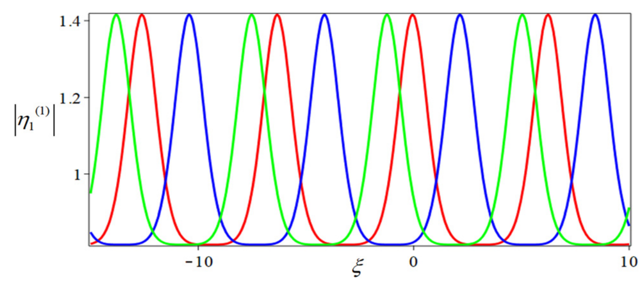

FIG. 16. The internal breathers at $\tau = 0$. Color in red: $\Psi_{10} = \Psi_{11} = \Psi_{12} = \sin(\tau)$, in blue: $\Psi_{10} = \Psi_{11} = \Psi_{12} = \tau$, and in green: $\Psi_{10} = 2$, $\Psi_{11} = \Psi_{12} = \sin(\tau)$.

C. Internal rogue waves

The phenomenon of oceanic rogue waves has attracted significant attention due to its irregular and sudden nature. However, there are relatively few physical models describing IRWs. In order to evaluate the ability of Eqs. (35)–(37) to describe IRWs and to investigate the influence of background flows, we choose

$$\begin{aligned} G &= n e^{\mathrm{i}a(\tau)}\{[px + \kappa py - \mathrm{i}\Omega(\tau) - \gamma_1] \\ &\quad \times [px + \kappa py + \mathrm{i}\Omega(\tau) + \gamma_1] + \gamma_2\}, \\ F &= [px + \kappa py - \mathrm{i}\Omega(\tau)][px + \kappa py + \mathrm{i}\Omega(\tau)] + \gamma_2, \end{aligned} \tag{56}$$

where n, p, κ, γ_1, and γ_2 are constants, while $a(\tau)$ and $\Omega(\tau)$ are functions solely dependent on τ.

Substituting Eq. (56) into Eqs. (40), we obtain the solution for IRWs

$$\eta_1^{(1)} = \frac{n e^{\mathrm{i}a(\tau)}\{[px + \kappa py - \mathrm{i}\Omega(\tau) - \gamma_1][px + \kappa py + \mathrm{i}\Omega(\tau) + \gamma_1] + \gamma_2\}}{[px + \kappa py - \mathrm{i}\Omega(\tau)][px + \kappa py + \mathrm{i}\Omega(\tau)] + \gamma_2}, \tag{57}$$

where

$$\begin{aligned} \gamma_2 &= \frac{\gamma_1^2}{4}, \quad a(\tau) = \int \frac{c_4(\tau) n^2 + c_9(\tau)}{c_1(\tau)} \mathrm{d}\tau, \\ \Omega(\tau) &= \int \frac{2p^2 [c_3(\tau)\kappa^2 + c_2(\tau)]}{\gamma_1 c_1(\tau)} \mathrm{d}\tau. \end{aligned} \tag{58}$$

The solutions for the upper and lower velocity potentials are given as follows:

$$\phi_1 = \alpha(\tau) \cdot \frac{2p(px + \kappa py)}{[px + \kappa py - \mathrm{i}\Omega(\tau)][px + \kappa py + \mathrm{i}\Omega(\tau)] + \frac{\gamma_1^2}{4}} + A, \tag{59}$$

$$\phi_2 = \beta(\tau) \cdot \frac{2p(px + \kappa py)}{[px + \kappa py - \mathrm{i}\Omega(\tau)][px + \kappa py + \mathrm{i}\Omega(\tau)] + \frac{\gamma_1^2}{4}} + B, \tag{60}$$

where

$$\alpha(\tau) = \frac{n^2 \gamma_1^2 [b_2(\tau) a_5(\tau) \kappa^2 + b_1(\tau) a_5(\tau) - b_5(\tau) a_3(\tau)]}{p^2[-a_2(\tau) b_2(\tau) \kappa^4 - a_2(\tau) b_1(\tau) \kappa^2 - a_1(\tau) b_2(\tau) \kappa^2 + b_3(\tau) a_3(\tau) - a_1(\tau) b_1(\tau)]}, \tag{61}$$

21 September 2024 04:25:04

Published under an exclusive license by AIP Publishing

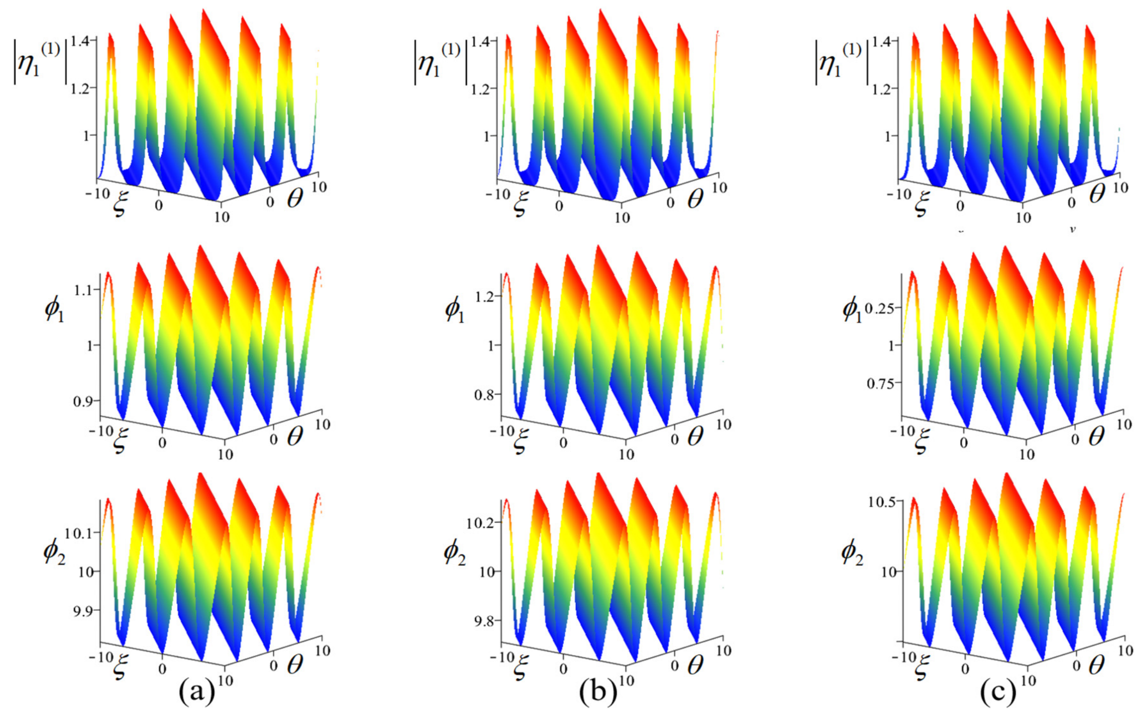

FIG. 17. Evolution of an internal breather and velocity potentials in the (ξ, θ) plane at time (a) $\tau = -15$, (b) $\tau = 0$, and (c) $\tau = 15$, respectively.

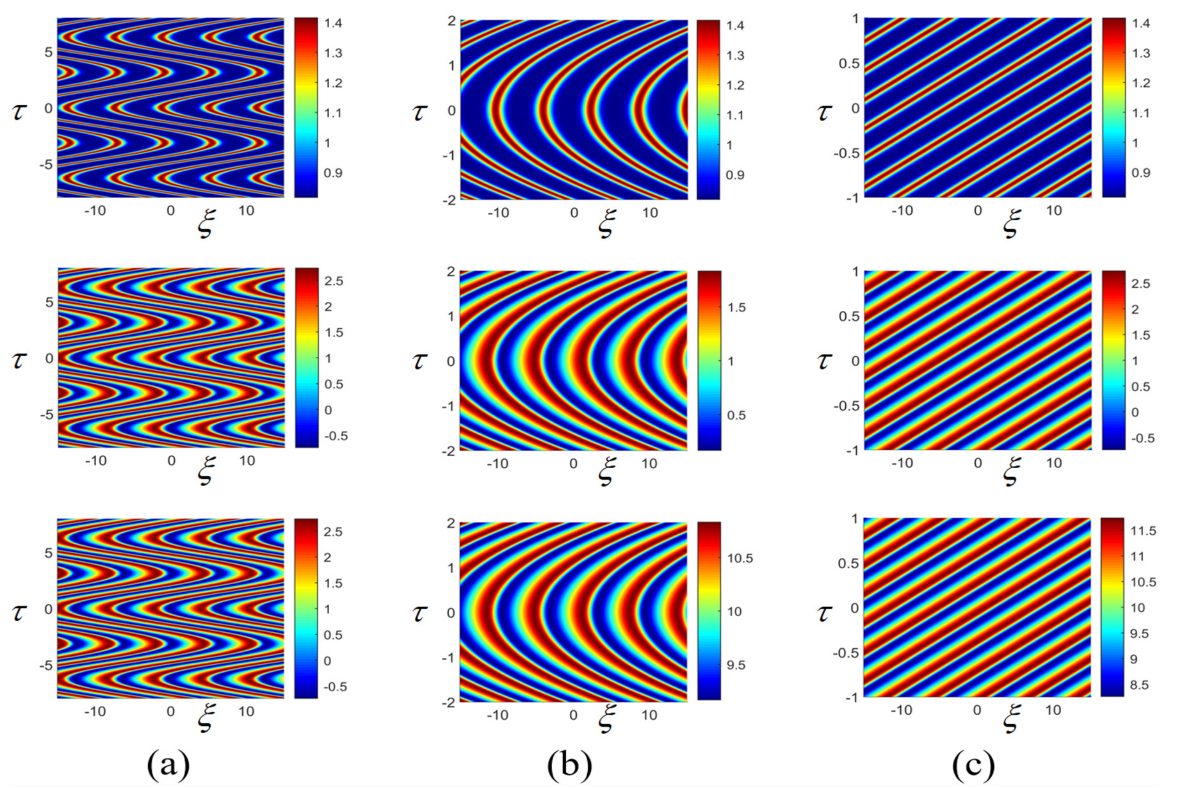

FIG. 18. The density plots of the internal breathers and the velocity potentials with $\Psi_{10} = 2$. (a) $\Psi_{11} = \Psi_{12} = \sin(\tau)$, (b) $\Psi_{11} = \Psi_{12} = \tau$, and (c) $\Psi_{11} = \Psi_{12} = 2$.

21 September 2024 04:25:04

Published under an exclusive license by AIP Publishing

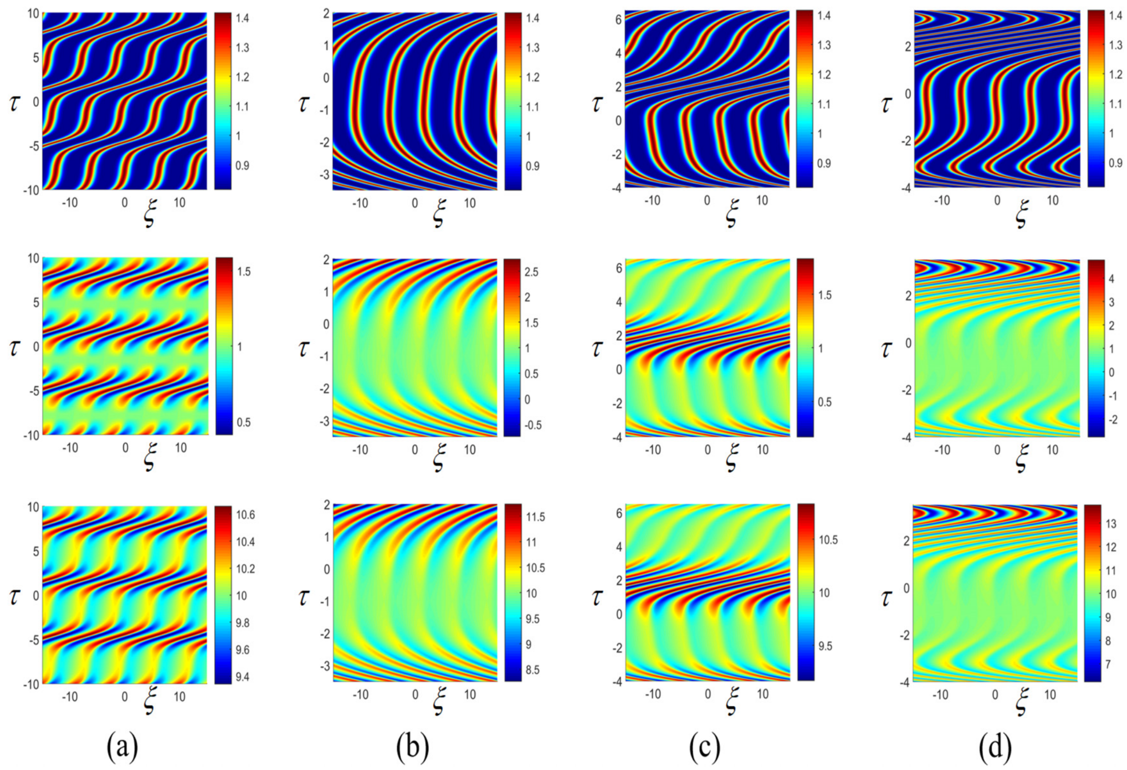

FIG. 19. The density plots of the internal breathers and the velocity potentials with $d_1 = d_2$. (a) $\Psi_{10} = \Psi_{11} = \Psi_{12} = \sin(\tau)$, (b) $\Psi_{10} = \Psi_{11} = \Psi_{12} = \tau$, (c) $\Psi_{10} = \sin(\tau)$, $\Psi_{11} = \Psi_{12} = \tau$, and (d) $\Psi_{10} = \tau$, $\Psi_{11} = \Psi_{12} = \sin(\tau)$.

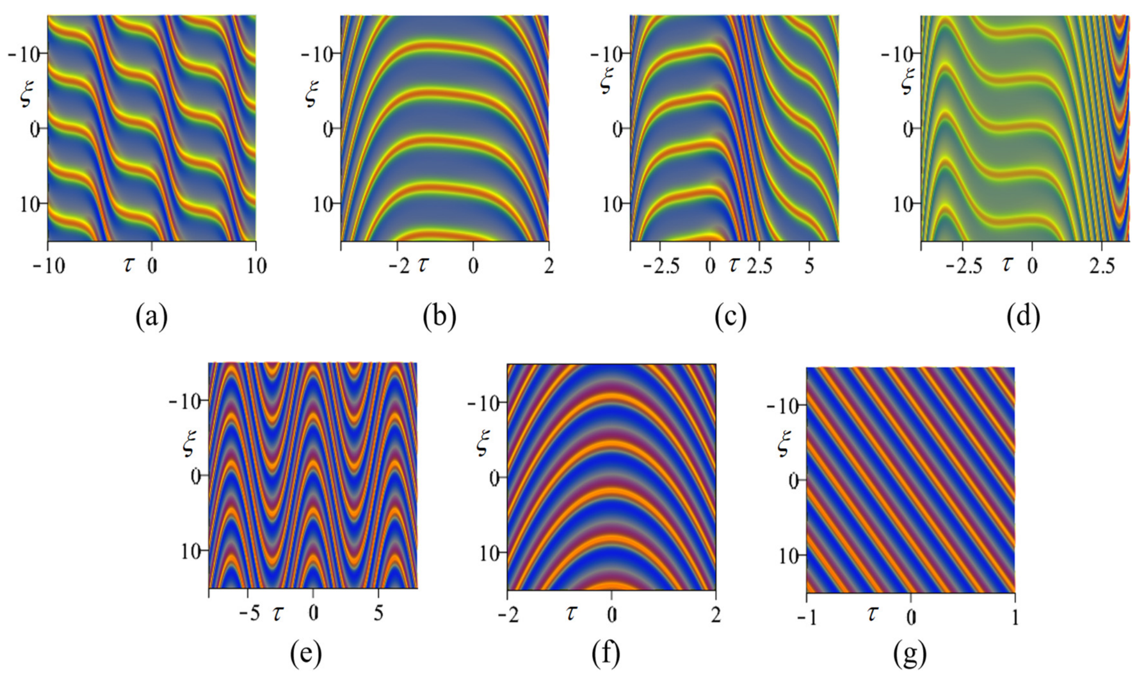

FIG. 20. The velocity potential indirectly infers the dynamic behaviors of internal breathers. (a) $\Psi_{10} = 2$, $\Psi_{11} = \Psi_{12} = \sin(\tau)$, (b) $\Psi_{10} = 2$, $\Psi_{11} = \Psi_{12} = \tau$, (c) $\Psi_{10} = \Psi_{11} = \Psi_{12} = 2$, (d) $\Psi_{10} = \Psi_{11} = \Psi_{12} = \sin(\tau)$, (e) $\Psi_{10} = \Psi_{11} = \Psi_{12} = \tau$, (f) $\Psi_{10} = \sin(\tau)$, $\Psi_{11} = \Psi_{12} = \tau$, and (g) $\Psi_{10} = \tau$, $\Psi_{11} = \Psi_{12} = \sin(\tau)$.

21 September 2024 04:25:04

Published under an exclusive license by AIP Publishing

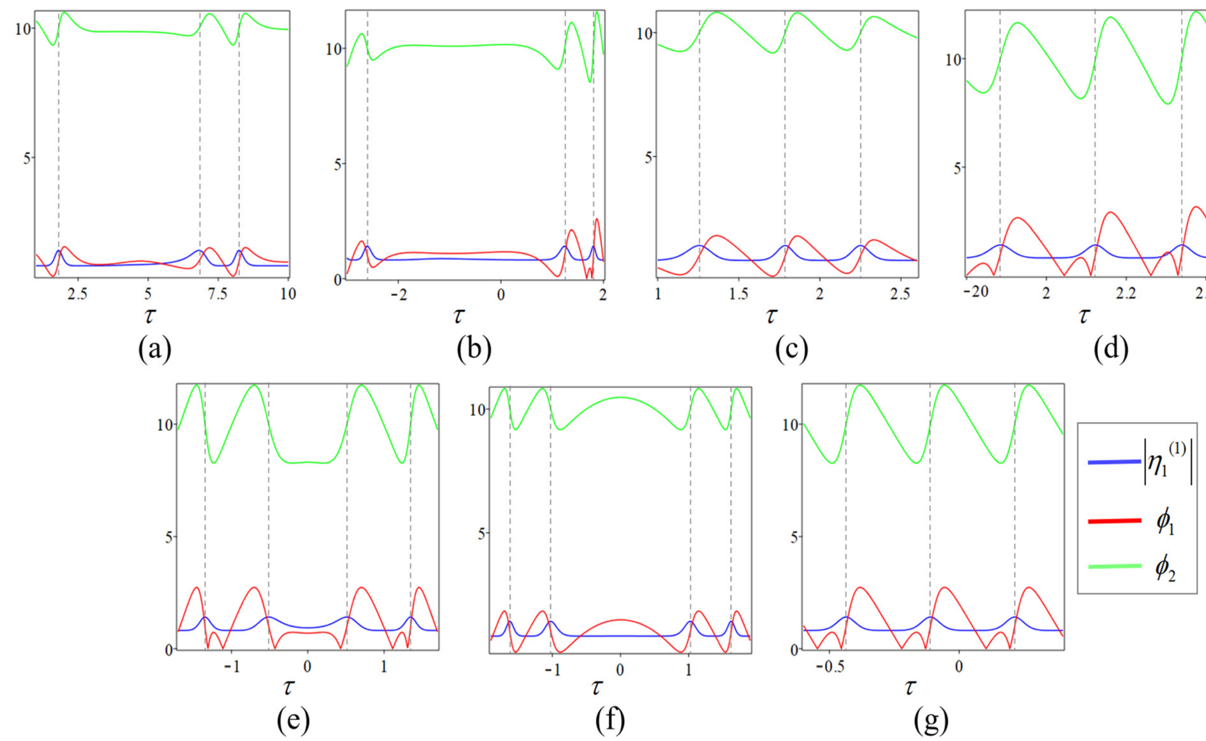

FIG. 21. The velocity potential indirectly infers the appearance of internal breathers. (a) $\Psi_{10} = 2$, $\Psi_{11} = \Psi_{12} = \sin(\tau)$, (b) $\Psi_{10} = 2$, $\Psi_{11} = \Psi_{12} = \tau$, (c) $\Psi_{10} = \Psi_{11} = \Psi_{12} = 2$, (d) $\Psi_{10} = \Psi_{11} = \Psi_{12} = \sin(\tau)$, (e) $\Psi_{10} = \Psi_{11} = \Psi_{12} = \tau$, (f) $\Psi_{10} = \sin(\tau)$, $\Psi_{11} = \Psi_{12} = \tau$, and (g) $\Psi_{10} = \tau$, $\Psi_{11} = \Psi_{12} = \sin(\tau)$.

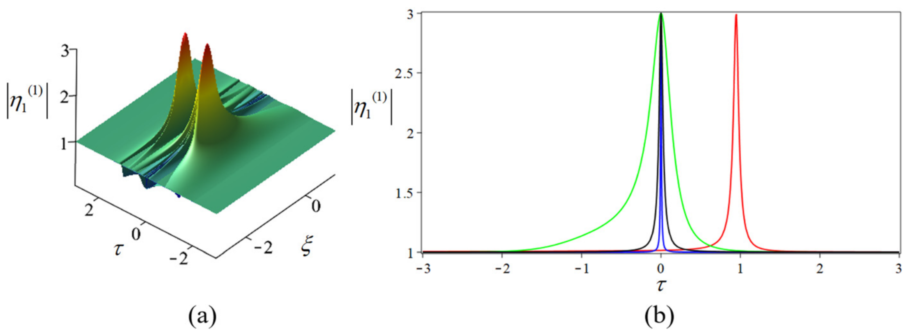

FIG. 22. The influence of background flows on the internal rogue waves. Color in red: $\Psi_{10} = \Psi_{11} = \Psi_{12} = \sin(\tau)$, in blue: $\Psi_{10} = \sin(\tau)$, $\Psi_{11} = \Psi_{12} = \tau$, in green: $\Psi_{10} = \Psi_{11} = \Psi_{12} = \tau$, and in black: $\Psi_{10} = 2$, $\Psi_{11} = \Psi_{12} = \tau$.

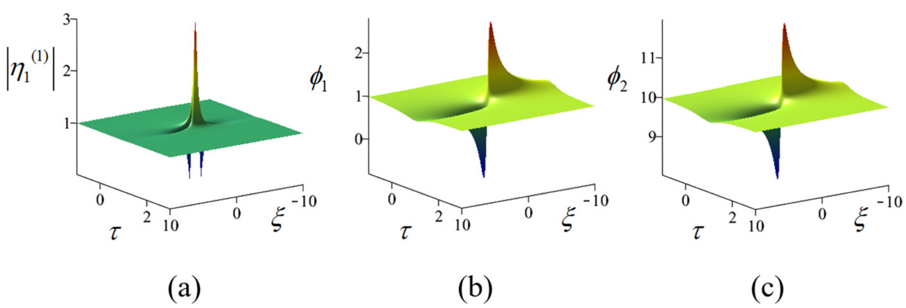

FIG. 23. Dynamical behavior of the internal rogue wave and velocity potentials with $d_1 = d_2$, $\Psi_{10} = \Psi_{11} = \Psi_{12} = \sin(\tau)$. (a) The internal rogue wave, (b) the upper-layer velocity potential ϕ_1, and (c) the lower-layer velocity potential ϕ_2.

21 September 2024 04:25:04

Published under an exclusive license by AIP Publishing

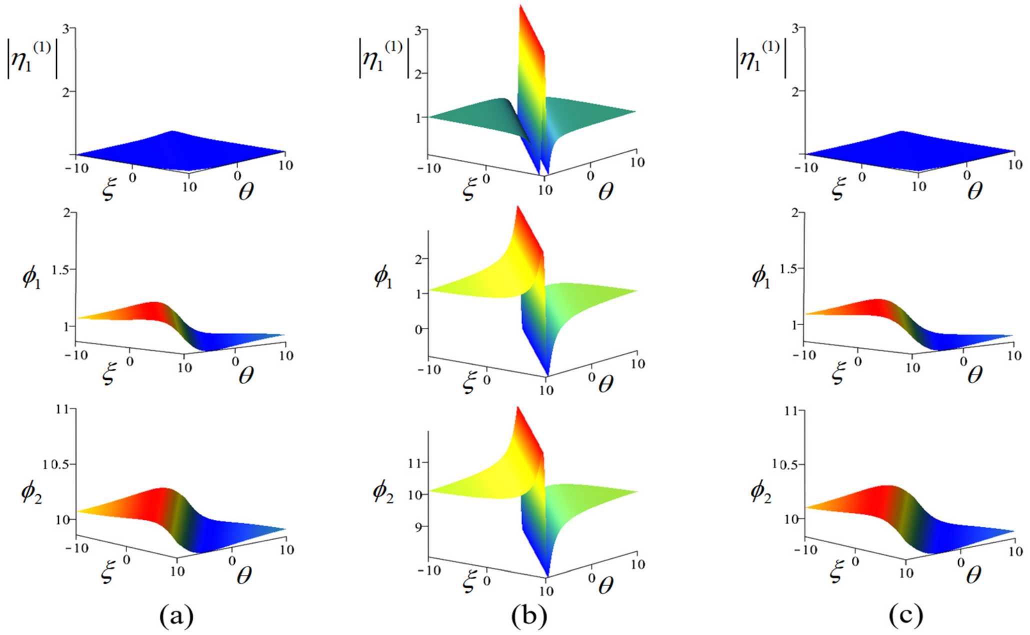

FIG. 24. Evolution of the internal rogue wave and velocity potentials in the $(\xi,\ \theta)$-plane at time (a) $\tau = -0.5$, (b) $\tau = 0.95$, and (c) $\tau = 1.3$, respectively.

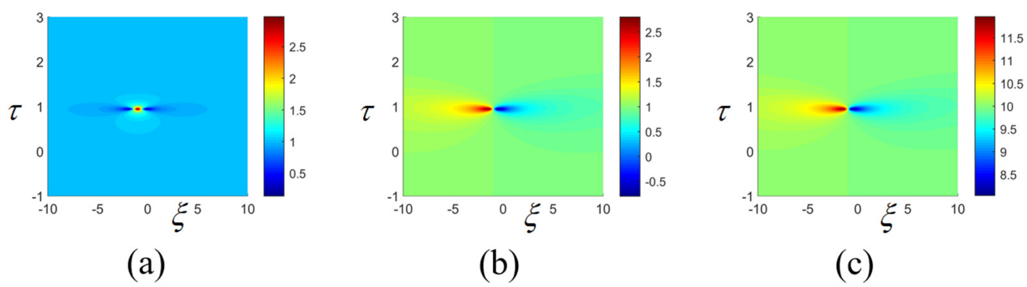

FIG. 25. The density plots of the internal rogue wave and the velocity potentials. (a) the internal rogue wave, (b) the upper-layer velocity potential ϕ_1, and (c) the lower-layer velocity potential ϕ_2.

$$\beta(\tau) = \frac{n^2\gamma_1^2\left[b_5(\tau)a_2(\tau)\kappa^2 + b_5(\tau)a_1(\tau) - b_3(\tau)a_5(\tau)\right]}{p^2\left[-a_2(\tau)b_2(\tau)\kappa^4 - a_2(\tau)b_1(\tau)\kappa^2 - a_1(\tau)b_2(\tau)\kappa^2 + b_3(\tau)a_3(\tau) - a_1(\tau)b_1(\tau)\right]}. \tag{62}$$

The conditions for describing IRWs with Eqs. (35)–(37) not only require $c_8 = 0$ but also need to satisfy $c_7 = 0$ (which has been verified to be feasible), indicating that additional limiting conditions may be necessary for the occurrence of rogue waves. As shown in Fig. 22, when the variations in the background flows are all periodic functions, IRWs no longer appear near $\tau = 0$ but instead around $\tau = 1$. As the primary variation in the background flows changes from $\sin(\tau)$ to 2 and then to τ, the duration of IRWs gradually increases. Different background flows affect the time interval when IRWs occur. The appearance time and duration of our IRWs vary due to changes in the background flows, though they resemble the internal rogue wave solutions obtained from the Gardner equation.[17] In Fig. 23, we only provide images of IRWs under a specific background flow [see Figs. 23(a)]. Compared to ISWs, the amplitude of IRWs is about three times greater, which increases energy and poses a serious threat to vessels and offshore structures. Moreover, IRWs exhibit localization in specific time regions, indicating significant energy concentration during propagation. This characteristic is also reflected in the changes of the velocity potentials, which show the impact of substantial energy accumulation on the surrounding fluid dynamic environment [see Figs. 23(b) and 23(c)].

Given the increased physical constraints required to obtain IRWs, and their sudden appearance and disappearance characteristics,

21 September 2024 04:25:04

Published under an exclusive license by AIP Publishing

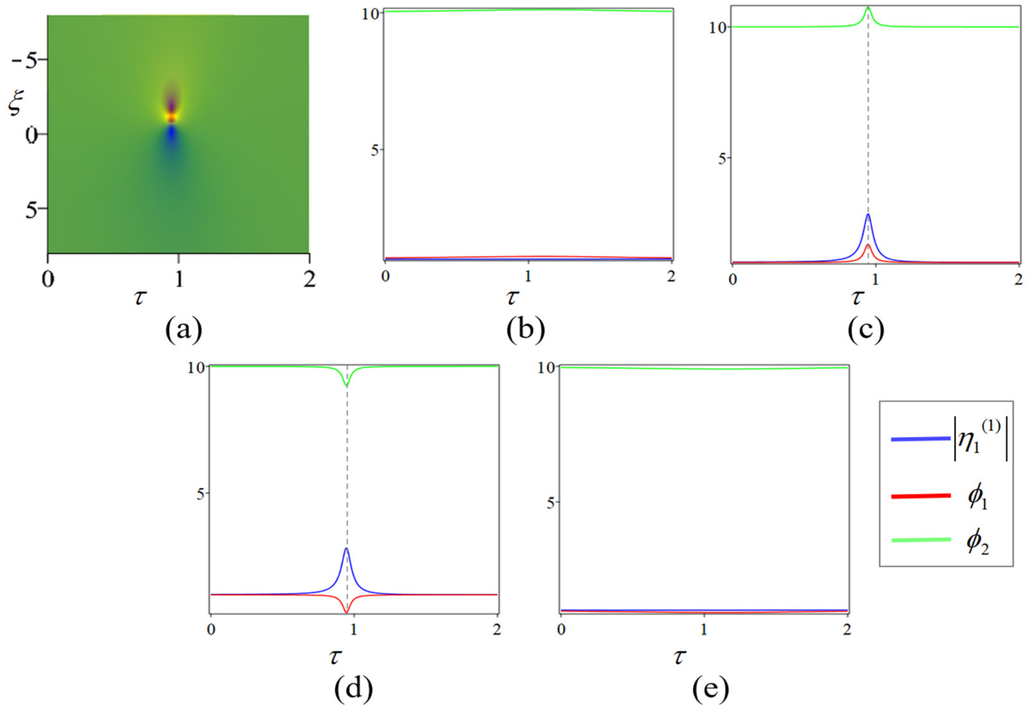

FIG. 26. The velocity potential indirectly infers the dynamic behavior and appearance of the internal rogue wave. (a) the dynamic behaviors of the internal rogue wave and the velocity potential; (b) $\xi = -20$, (c) $\xi = -1.1$, (d) $\xi = -0.9$, and (e) $\xi = 20$.

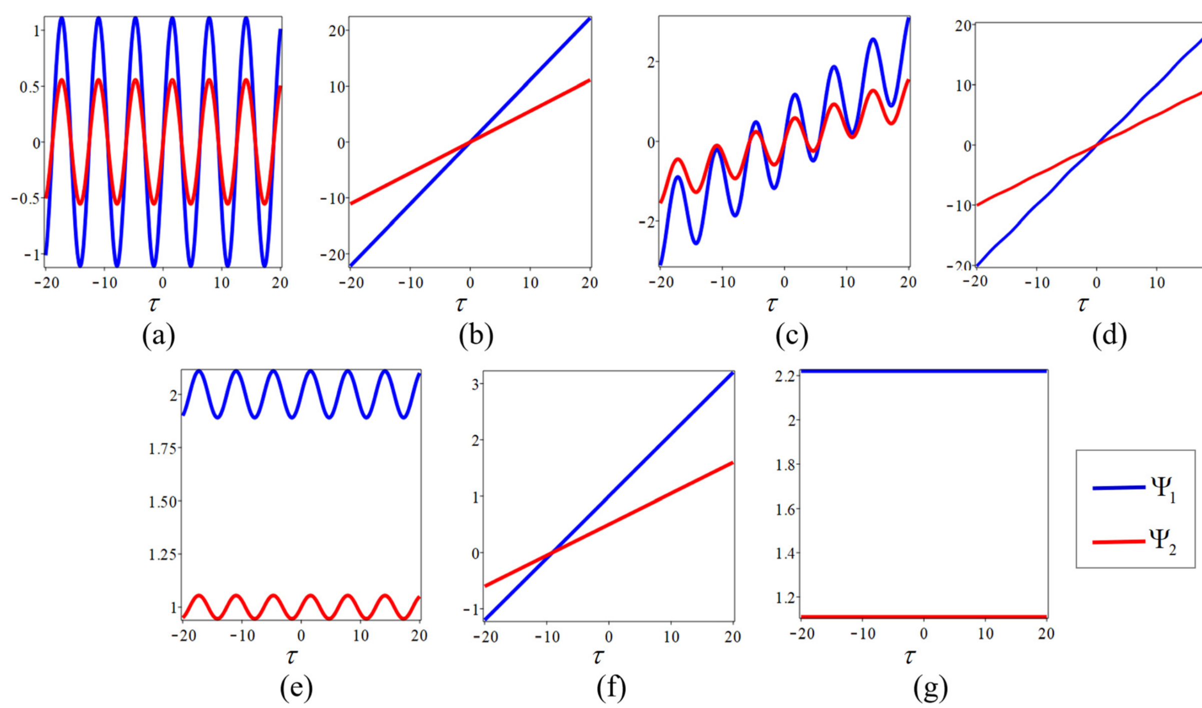

FIG. 27. The patterns of the background flows. (a) $\Psi_{10} = \Psi_{11} = \Psi_{12} = \sin(\tau)$, (b) $\Psi_{10} = \Psi_{11} = \Psi_{12} = \tau$, (c) $\Psi_{10} = \sin(\tau)$, $\Psi_{11} = \Psi_{12} = \tau$, (d) $\Psi_{10} = \tau$, $\Psi_{11} = \Psi_{12} = \sin(\tau)$, (e) $\Psi_{10} = 2$, $\Psi_{11} = \Psi_{12} = \sin(\tau)$, (f) $\Psi_{10} = 2$, $\Psi_{11} = \Psi_{12} = \tau$, and (g) $\Psi_{10} = \Psi_{11} = \Psi_{12} = 2$.

Published under an exclusive license by AIP Publishing

21 September 2024 04:25:04

capturing and detecting them becomes extremely challenging. In this case, can we utilize the changes in velocity potentials to indirectly detect IRWs? As shown in Fig. 24, images of IRWs at different time are presented. At the moment when IRWs just appear and are about to disappear [see Figs. 24(a) and 24(c)], the differences in velocity potentials in space are not significant. However, at the moment when the amplitude of the internal rogue wave reaches its peak [see Fig. 24(b)], there are greater differences in velocity potentials. This suggests a connection between the generation of large amplitudes and velocity potentials. Figures 25 and 26(a) demonstrate that changes in velocity potentials only occur in the region where IRWs appear. Similarly, in the two-dimensional Figs. 26(b)–26(e), velocity potentials do not changeover time when IRWs are absent, while in the time region when IRWs occur, there are noticeable changes in velocity potentials. Therefore, by monitoring changes in velocity potentials in the flow field, we may be able to infer the existence and characteristics of IRWs, thus better understand and utilize this complex fluid phenomenon in practical applications.

Finally, we integrate all variations of the background flows and provide images of the background flows under different patterns (see Fig. 27). Although the characteristics of the background flows under different modes are similar, for example, Figs. 27(b), 27(d), 27(f), and 27(g) exhibits linear characteristics, while Figs. 27(a), 27(c), and 27(e) shows periodic characteristics, the degree to which IWs are affected varies appreciably. Therefore, even minor changes in the background flows can markedly affect the response of IWs, emphasizing the importance of understanding the background flows for the dynamic behavior of IWs.

IV. CONCLUSIONS AND DISCUSSIONS

A novel variable-coefficient DS-type system is proposed for describing internal wave phenomena in stratified fluids with background flows. Considering the time dependence of the background flows, the system generates variable-coefficient terms and additional terms. When the background flows are time-independent, the system degenerates into a constant-coefficient form. We rely on this system to investigate the effects of the background flows on the dynamic behaviors of internal waves. Furthermore, this system not only has the capability to describe various high-dimensional internal waves but also captures the variations in the velocity potentials, aiding our investigation into the relation between the two.

We successfully derive precise solutions for ISWs, IBs, and IRWs, and investigate the effects of different patterns of background flows on IWs under two conditions: the primary variation terms of the background flows are constants, and the depths of the fluid upper and lower layers are equal. The results reveal that when the background flows are constant, the dynamical behaviors of ISWs and IBs align with those described for internal waves in previous models. However, when considering background flows with different temporal variations, ISWs and IBs exhibit various distinct dynamical behaviors. Both the primary and secondary variations significantly influence these behaviors, leading to irregular dynamic behaviors rarely reported before. In addition, it is observed that the influence of background flows on the dynamic behaviors of ISWs and IBs exhibits a certain consistency. At a fixed moment in time, the background flows have no effect on the amplitude of the ISWs and IBs, but change the spatial location where the ISWs and IBs appear. As for IRWs, they are subject to stricter physical constraints, with larger amplitudes and appearing only within specific time intervals. Different background flow patterns can influence the appearance time and duration of IRWs, suggesting that background flows are involved in the temporal modulation of these waves. This finding can aid in the prediction of IRWs. While past research primarily focused on the influence of background flows on amplitude, the above results emphasize that background flows also play a crucial role in the dynamics of IWs.

The research suggests that velocity potentials can reflect the dynamic behaviors of IWs under the influence of background flows and indirectly infer the spatiotemporal locations where internal wave amplitudes occur, thereby determining the type of IWs. This helps to compensate for the limitations of satellite imaging technology, providing valuable insights for detecting and identifying internal wave phenomena in practical applications. Additionally, with deep learning showing tremendous potential in fields such as fluid dynamics, oceanography, and atmospheric science, future research explores the application of deep learning to obtain more internal wave solutions of VCEDS system. Given the significant impact of background flows on internal waves, we would also aim to integrate inverse problem techniques from deep learning to discover parameters like background flow.

ACKNOWLEDGMENTS

This work was supported by the National Natural Science Foundation of China (Grants Nos. 12275085, 12235007, and 12175069) and Science and Technology Commission of Shanghai Municipality (Grant Nos. 21JC1402500 and 22DZ2229014).

AUTHOR DECLARATIONS

Conflict of Interest

The authors have no conflicts to disclose.

Author Contributions

Jun-Chao Sun: Methodology (lead); Software (lead); Writing—original draft (lead); Writing—review & editing (equal). **Xiao-Yan Tang:** Project administration (lead); Supervision (lead); Writing—review & editing (equal). **Yong Chen:** Project administration (lead); Supervision (lead); Writing—review & editing (equal).

DATA AVAILABILITY

Data sharing is not applicable to this article as no datasets were generated or analyzed during the current study.

APPENDIX: COEFFICIENTS OF THE VARIABLE-COEFFICIENT EXTENDED DS SYSTEM FOR INTERNAL WAVES

$$a_1(\tau) = \frac{(\rho_1 - \rho_2)d_1}{\delta h\left(U_r\delta\Psi_{10}(\tau) - C_g\right)} + \frac{\rho_1\left(U_r\delta\Psi_{10}(\tau) - C_g\right)}{\delta}, \tag{A1}$$

$$a_2(\tau) = \frac{(\rho_1 - \rho_2)d_1}{h\left(U_r\delta\Psi_{10}(\tau) - C_g\right)\delta}, \quad a_3(\tau) = -\frac{\rho 2\left(U_r\Psi_{20}(\tau)\delta - C_g\right)}{\delta}, \tag{A2}$$

Published under an exclusive license by AIP Publishing
21 September 2024 04:25:04

$$a_4(\tau) = -\frac{12(\rho_1-\rho_2)U_r\delta h^3(\Psi_{10}(\tau)kU_r\delta-\omega)}{(U_r\delta\Psi_{10}(\tau)-C_g)d_1(d_1^2k^2\delta+6h^2)k} + \frac{36U_r\rho_1h^6(\Psi_{10}(\tau)kU_r\delta-\omega)^2}{d_1^2(d_1^2k^2\delta+6h^2)^2k^2} - \frac{36U_r\rho_2h^6(\Psi_{20}(\tau)kU_r\delta-\omega)^2}{d2^2k^2(d2^2k^2\delta+6h^2)^2}, \tag{A3}$$

$$b_1(\tau) = -\frac{(\rho_1-\rho_2)d_2}{h\delta(U_r\Psi_{20}(\tau)\delta-C_g)} - \frac{\rho_2(U_r\Psi_{20}(\tau)\delta-C_g)}{\delta}, \tag{A4}$$

$$b_2(\tau) = -\frac{(\rho_1-\rho_2)d_2}{h(U_r\Psi_{20}(\tau)\delta-C_g)\delta}, \quad b_3(\tau) = \frac{\rho_1(U_r\delta\Psi_{10}(\tau)-C_g)}{\delta}, \tag{A5}$$

$$b_4(\tau) = \frac{12(\rho_1-\rho_2)U_r\delta h^3(\Psi_{20}(\tau)kU_r\delta-\omega)}{(U_r\Psi_{20}(\tau)\delta-C_g)d_2k(d_2^2k^2\delta+6h^2)} + \frac{36U_r\rho_1h^6(\Psi_{10}(\tau)kU_r\delta-\omega)^2}{d_1^2(d_1^2k^2\delta+6h^2)^2k^2} - \frac{36U_r\rho_2h^6(\Psi_{20}(\tau)kU_r\delta-\omega)^2}{d_2^2k^2(d_2^2k^2\delta+6h^2)^2}, \tag{A6}$$

$$\begin{aligned} c_1(\tau) = {} & \frac{1}{2}(d_1^2\delta h^2\rho_1+2h^2\rho_1)R_1(\tau) - R_2(\tau)\rho_2\left(\frac{1}{2}d_2^2h^2\delta+h^2\right) + \frac{1}{d_1^3\delta h^3+6d_1h^2k}6\rho_1\left(U_r\Psi_{10}(\tau)k\delta h^2 - \left(\frac{d_1^2h^2\delta}{2}+h^2\right)\omega\right)h^3 \\ & + \frac{1}{d_2^3\delta h^3+6d_2h^2k}6\rho_2\left(U_r\Psi_{20}(\tau)k\delta h^2 - \omega\left(\frac{1}{2}d_2^2h^2\delta+h^2\right)\right)h^3, \end{aligned} \tag{A7}$$

$$\begin{aligned} c_2(\tau) = {} & \left(-\frac{1}{2}\rho_1\delta(2kC_g+\omega)d_1^2R_1(\tau) + \frac{1}{2}\delta d_2^2\rho_2(2kC_g+\omega)R_2(\tau) + \left(U_r\Psi_{20}(\tau)\delta h^2 - h^2C_g - \left(\frac{kC_g}{2}+\omega\right)k\delta d_2^2\right)\rho_2F_1(\tau)\right. \\ & - \rho_1\left(\Psi_{10}(\tau)U_r\delta h^2 - h^2C_g - \left(\frac{kC_g}{2}+\omega\right)kd_1^2\delta\right)S_1(\tau) - W_1(\tau)h^2(\rho_1-\rho_2) + \frac{1}{d_1^3\delta k^3+6d_1h^2k} - \rho_1\left(U_r\Psi_{10}(\tau)k\delta h^2 - \left(\frac{d_1^2h^2\delta}{2}+h^2\right)\omega\right) \\ & \times\left(6\Psi_{10}(\tau)W_1(\tau)U_r\delta h^3 + 3R_1(\tau)d_1^3\delta k - 6W_1(\tau)h^3C_g - 6S_1(\tau)\left(\frac{d_1^2h^2\delta}{2}+h^2\right)d_1\right) - \frac{1}{d_2^3\delta h^3+6d_2h^2k} \\ & -\left(U_r\Psi_{20}(\tau)k\delta h^2 - \omega\left(\frac{d_2^2h^2\delta}{2}+h^2\right)\right)\rho_2\left(-6\Psi_{20}(\tau)W_1(\tau)U_r\delta h^3 + 3R_2(\tau)d_2^3\delta k + 6W_1(\tau)h^3C_g - 6\left(\frac{d_2^2h^2\delta}{2}+h^2\right)F_1(\tau)d_2\right), \end{aligned} \tag{A8}$$

$$\begin{aligned} c_3(\tau) = {} & -\frac{1}{2}(R_1(\tau)d_1^2\rho_1 - R_2(\tau)d_2^2\rho_2)\delta\omega - \frac{1}{d_1^3\delta k^3+6d_1h^2k}\rho_1\left(U_r\Psi_{10}(\tau)k\delta h^2 - \left(\frac{d_1^2h^2\delta}{2}+h^2\right)\omega\right)\left(R_1(\tau)d_1^3\delta k - 6\left(\frac{d_1^2h^2\delta}{6}+h^2\right)J_1(\tau)d_1\right) \\ & + \frac{1}{d_2^3\delta k^3+6d_2h^2k}\left(U_r\Psi_{20}(\tau)k\delta h^2 - \omega\left(\frac{d_2^2k^2\delta}{2}+h^2\right)\right)\rho_2\left(R_2(\tau)d_2^3\delta k - 6J_2(\tau)\left(\frac{d_2^2k^2\delta}{6}+h^2\right)d_2\right), \end{aligned} \tag{A9}$$

$$\begin{aligned} c_7(\tau) = {} & U_r\delta h^2\rho_1\Psi_{11}(\tau)R_1(\tau) - U_r\delta h^2\rho_2\Psi_{21}(\tau)R_2(\tau) + F_1(\tau)\Psi_{21}(\tau)U_r\delta h^2k\rho_2 - \left(U_r\Psi_{20}(\tau)\delta h^2 - h^2C_g - \left(\frac{1}{2}kC_g+\omega\right)k\delta d_2^2\right)\rho_2F_2(\tau) \\ & - S_1(\tau)\Psi_{11}(\tau)U_r\delta h^2k\rho_1 + \rho_1\left(\Psi_{10}(\tau)U_r\delta h^2 - h^2C_g - \left(\frac{1}{2}kC_g+\omega\right)kd_1^2\delta\right)S_2(\tau) + h^2W_2(\tau)(\rho_1-\rho_2) \\ & + \frac{1}{d_1^3\delta h^3+6d_1h^2k}\rho_1\left(U_r\Psi_{10}(\tau)k\delta h^2 - \left(\frac{1}{2}d_1^2k^2\delta+h^2\right)\omega\right)\left(-6\delta U_rh^3(W_1(\tau)k-1)\Psi_{11}(\tau) + 6h^3W_2(\tau)U_r\delta\Psi_{10}(\tau)\right. \\ & \left. - 6h^3C_gW_2(\tau) - 6S_2(\tau)\left(\frac{1}{2}d_1^2h^2\delta+h^2\right)d_1\right) - \frac{1}{d_2^3\delta h^3+6d_2h^2k}\left(U_r\Psi_{20}(\tau)k\delta h^2 - \omega\left(\frac{1}{2}d_2^2h^2\delta+h^2\right)\right)\rho_2 \\ & \times\left(6\delta U_rh^3(W_1(\tau)k-1)\Psi_{21}(\tau) - 6h^3W_2(\tau)U_r\delta\Psi_{20}(\tau) + 6h^3C_gW_2(\tau) - 6\left(\frac{1}{2}d_2^2h^2\delta+h^2\right)F_2(\tau)d_2\right), \end{aligned} \tag{A10}$$

$$\begin{aligned} c_4(\tau) = {} & \left(\frac{-1}{d_1^3\delta k^3+6d_1h^2k}6\rho_1\left(U_r\Psi_{10}(\tau)k\delta h^2 - \left(\frac{d_1^2\delta h^2}{2}+h^2\right)\omega\right)h^3\delta R_1(\tau)U_rk + \frac{-1}{d_2^3\delta h^3+6d_2h^2k}6\left(U_r\Psi_{20}(\tau)k\delta h^2\right.\right. \\ & \left.\left. - \omega\left(\frac{d_2^2h^2\delta}{2}+h^2\right)\right)\rho_2\delta U_rR_2(\tau)kh^3\right)B3(\tau) + \frac{-1}{d_1^3\delta k^3+6d_1h^2k}6\rho_1\left(U_r\Psi_{10}(\tau)k\delta h^2 - \left(\frac{d_1^2\delta h^2}{2}+h^2\right)\omega\right)h^3P1(\tau)kU_r\delta \\ & + \frac{-1}{d_2^3\delta k^3+6d_2h^2k}6\left(U_r\Psi_{20}(\tau)k\delta h^2 - \omega\left(\frac{d_2^2h^2\delta}{2}+h^2\right)\right)\rho_2M_1(\tau)kU_r\delta h^3 - R_1(\tau)P1(\tau)U_r\delta h^2k\rho_1 + R_2(\tau)M_1(\tau)U_r\delta h^2k\rho2 \\ & + \frac{-1}{d_1^3\delta k^3+6d_1h^2k}6\rho_1\left(U_r\Psi_{10}(\tau)k\delta h^2 - \left(\frac{d_1^2\delta h^2}{2}+h^2\right)\omega\right)R_1(\tau)G_1(\tau)U_r\delta h^3k \\ & + \frac{-1}{d_2^3\delta k^3+6d_2h^2k}6\left(U_r\Psi_{20}(\tau)k\delta h^2 - \omega\left(\frac{d_2^2h^2\delta}{2}+h^2\right)\right)\rho_2R_2(\tau)G_1(\tau)U_r\delta h^3k, \end{aligned} \tag{A11}$$

21 September 2024 04:25:04

Published under an exclusive license by AIP Publishing

$$c_5(\tau) = \left(\frac{-6\rho_1\left(U_r\Psi_{10}(\tau)k\delta h^2 - \left(\frac{d_1^2\delta h^2}{2}+h^2\right)\omega\right)h^3\delta R_1(\tau)U_r k}{d_1^3\delta k^3 + 6d_1h^2k} + \frac{-6\left(U_r\Psi_{20}(\tau)k\delta h^2 - \omega\left(\frac{d_2^2h^2\delta}{2}+h^2\right)\right)\rho_2\delta U_r R_2(\tau)kh^3}{d_2^3\delta k^3+6d_2h^2k}\right)B_1(\tau)$$
$$- U_r\delta R_1(\tau)\rho_1h^2k + \frac{-6\rho_1\left(U_r\Psi_{10}(\tau)k\delta h^2 - \left(\frac{d_1^2\delta h^2}{2}+h^2\right)\omega\right)h^3\delta U_r k}{d_1^3\delta k^3+6d_1h^2k}, \tag{A12}$$

$$c_6(\tau) = \left(\frac{-6\rho_1\left(U_r\Psi_{10}(\tau)k\delta h^2 - \left(\frac{d_1^2\delta k^2}{2}+h^2\right)\omega\right)h^3\delta R_1(\tau)U_r k}{d_1^3\delta h^3 + 6d_1h^2k} + \frac{-6\left(U_r\Psi_{20}(\tau)k\delta h^2 - \omega\left(\frac{d_2^2k^2\delta}{2}+h^2\right)\right)\rho_2\delta U_r R_2(\tau)kh^3}{d_2^3\delta k^3+6d_2h^2k}\right)B_2(\tau)$$
$$+ U_r\delta R_2(\tau)\rho_2h^2k + \frac{-6\left(U_r\Psi_{20}(\tau)k\delta h^2 - \omega\left(\frac{d_2^2h^2\delta}{2}+h^2\right)\right)\rho_2\delta U_r kh^3}{d_2^3\delta k^3+6d_2h^2k}, \tag{A13}$$

$$c_8(\tau) = \left(\frac{1}{2}d_1^2\delta h^2\rho_1 + h^2\rho_1\right)\left(\frac{\mathrm{d}}{\mathrm{d}\tau}R_1(\tau)\right) + \left(-\frac{1}{2}d_2^2k^2\delta\rho_2 - h^2\rho_2\right)\left(\frac{\mathrm{d}}{\mathrm{d}\tau}R_2(\tau)\right), \tag{A14}$$

$$\begin{aligned}c_9(\tau) = {}& U_r\delta(F_2(\tau)\Psi_{21}(\tau)\rho2 - \Psi_{12}(\tau)\rho_1R_1(\tau) + \Psi_{22}(\tau)\rho_2R_2(\tau) - S_2(\tau)\Psi_{11}(\tau)\rho_1)h^2k\\ &- \frac{6\rho_1\left(U_r\Psi_{10}(\tau)k\delta h^2 - \left(\frac{1}{2}d_1^2\delta k^2+h^2\right)\omega\right)h^3\delta(W_2(\tau)\Psi_{11}(\tau)+\Psi_{12}(\tau))U_r k}{d_1^3\delta k^3+6d_1h^2k}\\ &- \frac{6\left(U_r\Psi_{20}(\tau)k\delta h^2 - \omega\left(\frac{1}{2}d_2^2k^2\delta+h^2\right)\right)\rho_2\delta U_r(W_2(\tau)\Psi_{21}(\tau)+\Psi_{22}(\tau))kh^3}{d_2^3\delta k^3+6d_2h^2k},\end{aligned} \tag{A15}$$

$$\begin{aligned}W_1(\tau) = {}& (1296d_2(-(1/6)d_1^2k^2\delta + h^2)U_r^2k^2\rho_1((1/6)d_2^2k^2\delta + h^2)^2\delta^2h^3\Psi_{10}(\tau)^2\\ &- 2592d_2U_rk^2((1/24)\delta^2C_gk^4d_1^4 + (5/12)h^2\delta C_gk^2d_1^2 + (1/6)h^2\delta\omega kd_1^2\\ &+ h^4C_g)\rho_1((1/6)d_2^2k^2\delta + h^2)^2\delta h\Psi_{10}(\tau) + 1296U_r^2k^2(-(1/6)d_2^2k^2\delta\\ &+ h^2)d_1\delta^2((1/6)d_1^2k^2\delta + h^2)^2h^3\rho_2\Psi_{20}(\tau)^2 - 2592U_rk^2d_1\delta((1/6)d_1^2k^2\delta\\ &+ h^2)^2h\rho_2((1/24)\delta^2C_gk^4d_2^4 + (5/12)h^2\delta C_gk^2d_2^2 + (1/6)h^2\delta\omega kd_2^2 + h^4C_g)\Psi_{20}(\tau)\\ &+ d_2^5d_1^5\delta^4(\rho_1-\rho_2)k^{10} + 6d_2^4(d_1\rho_2 + d_2\rho_1)C_gd_1^4\omega\delta^4hk^9 + 12d_2^3((d_1^2+d_2^2)(\rho_1-\rho_2)h\\ &- (1/4)\delta\omega^2d_1d_2(d_1\rho_2 + d_2\rho_1))d_1^3\delta^3hk^8 + 48d_2^2C_g(d_1^3\rho_2 + ((3/2)(d_1^2))d_2\rho_1\\ &+ ((3/2)d_1)d_2^2\rho_2 + d_2^3\rho_1)d_1^2\omega\delta^3h^3k^7 + 36d_2d_1\delta^2((d_1^4 + 4d_1^2d_2^2 + d_2^4)(\rho_1-\rho_2)h\\ &- \delta\omega^2d_1^2d_2^2(d_1\rho_1 + d_2\rho_2))h^3k^6 + (72(d_1^5\rho_2 + 3d_1^4d_2\rho_1 + 8d_1^3d_2^2\rho_2 + 8d_1^2d_2^3\rho_1\\ &+ 3d_1d_2^4\rho_2 + d_2^5\rho_1))C_g\omega\delta^2h^5k^5 + (432(d_1d_2(d_1^2+d_2^2)(\rho_1-\rho_2)h\\ &- (1/12)\delta\omega^2(d_1^5\rho_2 + 3d_1^4d_2\rho_1 + 3d_1d_2^4\rho_2 + d_2^5\rho_1)))\delta h^5k^4 + (864(d_1^3\rho_2 + 2d_1^2d_2\rho_1\\ &+ 2d_1d_2^2\rho_2 + d_2^3\rho_1))C_g\omega\delta h^7k^3 + (1296(d_1d_2(\rho_1-\rho_2)h - (1/3)\delta\omega^2(d_1^3\rho_2\\ &+ d_2^3\rho_1)))h^7k^2 + (2592(d_1\rho_2 + d_2\rho_1))C_g\omega h^9k - (1296(d_1\rho_2 + d_2\rho_1))\omega^2h^9)/\\ &((1296((1/6)d_1^2k^2\delta + h^2))((1/6)d_2^2k^2\delta + h^2)k(h^3\delta^2k^2U_r^2d_2\rho_1((1/6)d_2^2k^2\delta\\ &+ h^2)\Psi_{10}(\tau)^2 - 2d_2U_r((1/4)d_1^2k^2\delta + h^2)k\rho_1((1/6)d_2^2k^2\delta + h^2)\omega\delta h\Psi_{10}(\tau)\\ &+ h^3\delta^2k^2U_r^2d_1\rho_2((1/6)d_1^2k^2\delta + h^2)\Psi_{20}(\tau)^2 - 2U_rkd_1\omega((1/4)d_2^2k^2\delta\\ &+ h^2)\delta((1/6)d_1^2k^2\delta + h^2)h\rho_2\Psi_{20}(\tau) + (1/36)d_1^3d_2^3\delta^2k^6(\rho_1-\rho_2) + (1/6)d_2((d_1^2\\ &+ d_2^2)(\rho_1-\rho_2)h + (1/2)\delta\omega^2d_1d_2(d_1\rho_2 + d_2\rho_1))d_1\delta hk^4 + (d_1d_2(\rho_1-\rho_2)h\\ &+ (1/6)\delta\omega^2(d_1^3\rho_2 + 3d_1^2d_2\rho_1 + 3d_1d_2^2\rho_2 + d_2^3\rho_1))h^3k^2 + h^5\omega^2(d_1\rho_2 + d_2\rho_1))),\end{aligned} \tag{A16}$$

$$R_1(\tau) = \frac{6h^3(U_r\Psi_{10}(\tau)k\delta - \omega)}{d_1(d_1^2\delta k^2 + 6h^2)k}, \quad R_2(\tau) = -\frac{6h^3(U_r\Psi_{20}(\tau)k\delta - \omega)}{d_2k(d_2^2\delta k^2 + 6h^2)}, \tag{A17}$$

$$J_1(\tau) = \frac{2h^2}{2U_r\Psi_{10}(\tau)k\delta h^2 - \omega d_1^2k^2\delta - 2\omega h^2}, \quad J_2(\tau) = \frac{2h^2}{2U_r\Psi_{20}(\tau)k\delta h^2 - \omega d_2^2k^2\delta - 2\omega h^2}, \tag{A18}$$

21 September 2024 04:25:04

Published under an exclusive license by AIP Publishing

$$
\begin{aligned}
W_2(\tau) = {} & -2U_r k\delta h(h^2\delta\Psi_{11}(\tau)kU_r d_2\rho_1((1/6)d_2^2k^2\delta + h^2)\Psi_{10}(\tau) + h^2\delta\Psi_{21}(\tau) \\
& \times kU_r d_1\rho_2((1/6)d_1^2k^2\delta + h^2)\Psi_{20}(\tau) - \omega(d_2((1/4)d_1^2k^2\delta + h^2)\rho_1((1/6)d_2^2k^2\delta \\
& + h^2)\Psi_{11}(\tau) + d_1\Psi_{21}(\tau)((1/4)d_2^2k^2\delta + h^2)((1/6)d_1^2k^2\delta + h^2)\rho_2))/ \\
& (h^3\delta^2k^2U_r^2d_2\rho_1((1/6)d_2^2k^2\delta + h^2)\Psi_{10}(\tau)^2 - 2d_2U_r((1/4)d_1^2k^2\delta + h^2)k\rho_1((1/6)d_2^2k^2\delta \\
& + h^2)\omega\delta h\Psi_{10}(\tau) + h^3\delta^2k^2U_r^2d_1\rho_2((1/6)d_1^2k^2\delta + h^2)\Psi_{20}(\tau)^2 - 2U_r kd_1\omega((1/4)d_2^2k^2\delta \\
& + h^2)\delta((1/6)d_1^2k^2\delta + h^2)h\rho_2\Psi_{20}(\tau) + (1/36)d_1^3d_2^3\delta^2k^6(\rho_1 - \rho_2) + (1/6)d_2((d_1^2 \\
& + d_2^2)(\rho_1 - \rho_2)h + (1/2)\delta\omega^2d_1d_2(d_1\rho_2 + d_2\rho_1))d_1\delta hk^4 + (d_1d_2(\rho_1 - \rho_2)h \\
& + (1/6)\delta\omega^2(d_1^3\rho_2 + 3d_1^2d_2\rho_1 + 3d_1d_2^2\rho_2 + d_2^3\rho_1))h^3k^2 + h^5\omega^2(d_1\rho_2 + d_2\rho_1)),
\end{aligned}
\tag{A19}
$$

$$
\begin{aligned}
S_2(\tau) = {} & -U_r\delta(h^3\delta^2\Psi_{11}(\tau)k^2U_r^2d_2\rho_1((1/6)d_2^2k^2\delta + h^2)\Psi_{10}(\tau)^2 \\
& + (2(h^2\delta\Psi_{21}(\tau)kU_r d_1\rho_2((1/6)d_1^2k^2\delta + h^2)\Psi_{20}(\tau) - (h^2d_2\rho_1((1/6)d_2^2k^2\delta + h^2)\Psi_{1,1}(\tau) \\
& + d_1\Psi_{21}(\tau)((1/4)d_2^2k^2\delta + h^2)((1/6)d_1^2k^2\delta + h^2)\rho_2)\omega))U_r k\delta h\Psi_{10}(\tau) \\
& - U_r^2\Psi_{1,1}(\tau)k^2d_1\delta^2((1/6)d_1^2k^2\delta + h^2)h^3\rho_2\Psi_{20}(\tau)^2 + 2U_r kd_1(((1/4)d_2^2k^2\delta + h^2)\Psi_{1,1}(\tau) \\
& - h^2\Psi_{21}(\tau))\omega\delta((1/6)d_1^2k^2\delta + h^2)h\rho_2\Psi_{20}(\tau) + (-(1/36)d_1^3d_2^3\delta^2k^6(\rho_1 - \rho_2) \\
& - (1/6)d_2((d_1^2 + d_2^2)(\rho_1 - \rho_2)h + (1/2)\delta\omega^2d_1^2d_2\rho_2)d_1\delta hk^4 - (d_1d_2(\rho_1 - \rho_2)h \\
& + (1/6)\delta\omega^2(d_1^3\rho_2 + 3d_1d_2^2\rho_2 - d_2^3\rho_1))h^3k^2 - h^5\omega^2(d_1\rho_2 - d_2\rho_1))\Psi_{1,1}(\tau) \\
& + 2d_1\Psi_{21}(\tau)\omega^2((1/4)d_2^2k^2\delta + h^2)((1/6)d_1^2k^2\delta + h^2)h\rho_2)h^3/((h^3\delta^2k^2U_r^2d_2\rho_1 \\
& \times ((1/6)d_2^2k^2\delta + h^2)\Psi_{10}(\tau)^2 - 2d_2U_r((1/4)d_1^2k^2\delta + h^2)k\rho_1((1/6)d_2^2k^2\delta + h^2)\omega\delta h\Psi_{10}(\tau) \\
& + h^3\delta^2k^2U_r^2d_1\rho_2((1/6)d_1^2k^2\delta + h^2)\Psi_{20}(\tau)^2 - 2U_r kd_1\omega((1/4)d_2^2k^2\delta + h^2)\delta((1/6)d_1^2k^2\delta \\
& + h^2)h\rho_2\Psi_{20}(\tau) + (1/36)d_1^3d_2^3\delta^2k^6(\rho_1 - \rho_2) + (1/6)d_2((d_1^2 + d_2^2)(\rho_1 - \rho_2)h \\
& + (1/2)\delta\omega^2d_1d_2(d_1\rho_2 + d_2\rho_1))d_1\delta hk^4 + (d_1d_2(\rho_1 - \rho_2)h + (1/6)\delta\omega^2(d_1^3\rho_2 + 3d_1^2d_2\rho_1 \\
& + 3d_1d_2^2\rho_2 + d_2^3\rho_1))h^3k^2 + h^5\omega^2(d_1\rho_2 + d_2\rho_1))d_1((1/6)d_1^2k^2\delta + h^2)),
\end{aligned}
\tag{A20}
$$

$$
\begin{aligned}
S_1(\tau) = {} & -(-d_2U_r^3k^2\rho_1((1/6)d_2^2k^2\delta + h^2)^2\delta^3h^3\Psi_{10}(\tau)^3 + 2d_2((1/2)kC_g + \omega)U_r^2k\rho_1 \\
& \times ((1/6)d_2^2k^2\delta + h^2)^2((1/2)d_1^2k^2\delta + h^2)\delta^2h\Psi_{10}(\tau)^2 + U_r(-U_r^2k^2d_1((1/36)\delta^2k^4d_1^2d_2^2 \\
& + (1/2)(d_1^2 - (1/3)d_2^2)\delta h^2k^2 + h^4)\delta^2h^3\rho_2\Psi_{20}(\tau)^2 + (2((1/144)d_1^2d_2^4\delta^3k^6C_g + (1/72) \\
& \times d_1^2d_2^4\delta^3k^5\omega + (1/72)(5(d_1^2 + 3d_2^2(1/5)))d_2^2C_g\delta^2h^2k^4 + (1/6)d_1^2d_2^2\delta^2h^2k^3\omega + (1/6)C_g(d_1^2 \\
& + 5d_2^2(1/2))\delta h^4k^2 + (1/3)(d_1^2 + (1/2)d_2^2)\omega\delta h^4k + h^6C_g))U_r k^2d_1\delta h\rho_2\Psi_{20}(\tau) \\
& - (1/72)\delta^3d_1^3d_2^5(\rho_1 - \rho_2)k^8 - (1/36)d_1^2d_2^4\delta^3h\omega C_g(d_1\rho_2 + d_2\rho_1)k^7 - (1/6)d_2^3((d_1^2 \\
& + (1/6)d_2^2)(\rho_1 - \rho_2)h + (1/12)\delta\omega^2d_1d_2(d_1\rho_2 + 4d_2\rho_1))d_1\delta^2hk^6 - 2d_2^2(d_1^3\rho_2 \\
& + ((3/2)(d_1^2))d_2\rho_1 + ((3/4)d_1)d_2^2\rho_2 + (1/4)d_2^3\rho_1)C_g\omega\delta^2h^3k^5(1/9) - (1/2)d_2((d_1^2 \\
& + 2d_2^2(1/3))d_1(\rho_1 - \rho_2)h + (1/9)(4(d_1^3\rho_2 + 3d_1^2d_2\rho_1 - (3/8d_1)d_2^2\rho_2 \\
& + (1/8)d_2^3\rho_1))d_2\omega^2\delta)\delta h^3k^4 - (1/3)\delta h^5\omega C_g(d_1^3\rho_2 + 3d_1^2d_2\rho_1 + 4d_1d_2^2\rho_2 + 2d_2^3\rho_1)k^3 \\
& - (d_1d_2(\rho_1 - \rho_2)h + (1/6)\delta\omega^2(d_1^3\rho_2 + 12d_1^2d_2\rho_1 + 2d_2^3\rho_1))h^5k^2 - 2h^7\omega C_g(d_1\rho_2 \\
& + d_2\rho_1)k + h^7\omega^2(d_1\rho_2 - d_2\rho_1))\delta\Psi_{10}(\tau) + 2U_r^2k(-(1/72)d_1^2d_2^2\delta^2k^5C_g \\
& + (1/36)\delta^2\omega k^4d_1^2d_2^2 - (1/12)h^2\delta C_g(d_1^2 + d_2^2)k^3 + (1/3)h^2\delta\omega k^2d_1^2 - (1/2)h^4kC_g \\
& + h^4\omega)d_1\delta^2h^3\rho_2\Psi_{20}(\tau)^2 - 2U_r((1/48)d_1^2d_2^4\delta^3k^6 + 17d_2^2(d_1^2 + 3d_2^2(1/17))\delta^2h^2k^4(1/72) \\
& + (1/2)(d_1^2 + 7d_2^2(1/6))\delta h^4k^2 + h^6)d_1\omega^2\delta h\rho_2\Psi_{20}(\tau) - (1/216)\delta^3d_1^3d_2^5C_g(\rho_1 - \rho_2)k^8 \\
& + (1/54)\delta^3d_1^3d_2^5\omega(\rho_1 - \rho_2)k^7 - (1/18)d_2^3C_gd_1\delta^2((d_1^2 + (1/2)d_2^2)(\rho_1 - \rho_2)h \\
& - (1/4)\delta\omega^2d_1d_2(d_1\rho_2 + d_2\rho_1))hk^6 + 2d_2^3((d_1^2 + (1/4)d_2^2)(\rho_1 - \rho_2)h + (1/8)\delta\omega^2d_1d_2(d_1\rho_2 \\
& + d_2\rho_1))d_1\omega\delta^2hk^5(1/9) - (1/6)d_2(d_1(d_1^2 + 2d_2^2)(\rho_1 - \rho_2)h - 2d_2(d_1^3\rho_2 + ((3/2)(d_1^2))d_2\rho_1 \\
& + ((3/4)d_1)d_2^2\rho_2 + (1/4)d_2^3\rho_1)\omega^2\delta(1/3))C_g\delta h^3k^4 + 2d_2((d_1^2 + d_2^2)(\rho_1 - \rho_2)h
\end{aligned}
$$

21 September 2024 04:25:04

Published under an exclusive license by AIP Publishing

$$
\begin{aligned}
&+ (1/2)\delta\omega^2 d_1 d_2(d_1\rho_2 + d_2\rho_1))d_1\omega\delta h^3 k^3(1/3) - C_g(d_1 d_2(\rho_1 - \rho_2)h - (1/6)\delta\omega^2(d_1^3\rho_2 \\
&+ 3d_1^2 d_2\rho_1 + 4d_1 d_2^2\rho_2 + 2d_2^3\rho_1))h^5k^2 + 2d_1\omega(d_2(\rho_1 - \rho_2)h + (1/6)\delta\omega^2(d_1^2\rho_2 + 3d_1 d_2\rho_1 \\
&+ 2d_2^2\rho_2))h^5k + h^7\omega^2 C_g(d_1\rho_2 + d_2\rho_1))h^3/((h^3\delta^2k^2U_r^2 d_2\rho_1((1/6)d_2^2k^2\delta + h^2)\Psi_{10}(\tau)^2 \\
&- 2d_2U_r((1/4)d_1^2k^2\delta + h^2)k\rho_1((1/6)d_2^2k^2\delta + h^2)\omega\delta h\Psi_{10}(\tau) + h^3\delta^2k^2U_r^2 d_1\rho_2((1/6)d_1^2k^2\delta \\
&+ h^2)\Psi_{20}(\tau)^2 - 2U_r k d_1\omega((1/4)d_2^2k^2\delta + h^2)\delta((1/6)d_1^2k^2\delta + h^2)h\rho_2\Psi_{20}(\tau) \\
&+ (1/36)d_1^3d_2^3\delta^2k^6(\rho_1 - \rho_2) + (1/6)d_2((d_1^2 + d_2^2)(\rho_1 - \rho_2)h + (1/2)\delta\omega^2 d_1 d_2(d_1\rho_2 \\
&+ d_2\rho_1))d_1\delta h k^4 + (d_1 d_2(\rho_1 - \rho_2)h + (1/6)\delta\omega^2(d_1^3\rho_2 + 3d_1^2 d_2\rho_1 + 3d_1 d_2^2\rho_2 + d_2^3\rho_1))h^3k^2 \\
&+ h^5\omega^2(d_1\rho_2 + d_2\rho_1))((1/6)d_1^2k^2\delta + h^2)((1/6)d_2^2k^2\delta + h^2)kd_1),
\end{aligned}
\tag{A21}
$$

$$
\begin{aligned}
F_1(\tau) = {}& h^3(-U_r^3k^2d_1\delta^3((1/6)d_1^2k^2\delta + h^2)^2h^3\rho_2\Psi_{20}(\tau)^3 + (2((1/2)kC_g + \omega))U_r^2k((1/2)d_2^2k^2\delta \\
&+ h^2)d_1\delta^2((1/6)d_1^2k^2\delta + h^2)^2h\rho_2\Psi_{20}(\tau)^2 - U_r(d_2U_r^2k^2((1/36)\delta^2k^4d_1^2d_2^2 - (1/6)\delta h^2(d_1^2 \\
&- 3d_2^2)k^2 + h^4)\rho_1\delta^2h^3\Psi_{10}(\tau)^2 - 2d_2U_rk^2\rho_1((1/144)d_1^4d_2^2\delta^3k^6C_g + (1/72)d_1^4d_2^2\delta^3k^5\omega \\
&+ (1/24)(d_1^2 + 5d_2^2(1/3))C_g d_1^2\delta^2h^2k^4 + (1/6)d_1^2d_2^2\delta^2h^2k^3\omega + 5C_g\delta(d_1^2 \\
&+ 2d_2^2(1/5))h^4k^2(1/12) + (1/6)\delta h^4\omega(d_1^2 + 2d_2^2)k + h^6C_g)\delta h\Psi_{10}(\tau) + (1/72)\delta^3d_1^5d_2^3(\rho_1 \\
&- \rho_2)k^8 + (1/36)d_1^4d_2^3\delta^3h\omega C_g(d_1\rho_2 + d_2\rho_1)k^7 + (1/36)d_2d_1^3((d_1^2 + 6d_2^2)(\rho_1 - \rho_2)h \\
&+ 2d_2d_1(d_1\rho_2 + (1/4)d_2\rho_1)\omega^2\delta)\delta^2hk^6 + (1/18)d_1^2\delta^2h^3\omega C_g(d_1^3\rho_2 + 3d_1^2d_2\rho_1 + 6d_1d_2^2\rho_2 \\
&+ 4d_2^3\rho_1)k^5 + (1/3)(d_2(d_1^2 + 3d_2^2(1/2))(\rho_1 - \rho_2)h + (1/12)d_1\delta\omega^2(d_1^3\rho_2 - 3d_1^2d_2\rho_1 \\
&+ 24d_1d_2^2\rho_2 + 8d_2^3\rho_1))d_1\delta h^3k^4 + (1/3)(2(d_1^3\rho_2 + 2d_1^2d_2\rho_1 + ((3/2)d_1)d_2^2\rho_2 \\
&+ (1/2)d_2^3\rho_1))C_g\omega\delta h^5k^3 + (d_1d_2(\rho_1 - \rho_2)h + (1/3)(d_1^3\rho_2 + 6d_1d_2^2\rho_2 \\
&+ (1/2)d_2^3\rho_1)\omega^2\delta)h^5k^2 + 2h^7\omega C_g(d_1\rho_2 + d_2\rho_1)k + h^7\omega^2(d_1\rho_2 - d_2\rho_1))\delta\Psi_{20}(\tau) \\
&+ 2d_2U_r^2k\rho_1(-(1/72)d_1^2d_2^2\delta^2k^5C_g + (1/36)\delta^2\omega k^4d_1^2d_2^2 - (1/12)h^2\delta C_g(d_1^2 + d_2^2)k^3 \\
&+ (1/3)h^2\delta\omega k^2d_2^2 - (1/2)h^4kC_g + h^4\omega)\delta^2h^3\Psi_{10}(\tau)^2 - 2d_2U_r\rho_1((1/48)d_1^4d_2^2\delta^3k^6 \\
&+ (1/24)(d_1^2 + 17d_2^2(1/3))d_1^2\delta^2h^2k^4 + 7\delta(d_1^2 + 6d_2^2(1/7))h^4k^2(1/12) + h^6)\omega^2\delta h\Psi_{10}(\tau) \\
&- (1/216)d_1^5d_2^3\delta^3C_g(\rho_1 - \rho_2)k^8 + (1/54)d_1^5d_2^3\delta^3\omega(\rho_1 - \rho_2)k^7 - (1/36)d_2((d_1^2 + 2d_2^2)(\rho_1 \\
&- \rho_2)h - (1/2)\delta\omega^2d_1d_2(d_1\rho_2 + d_2\rho_1))C_g d_1^3\delta^2hk^6 + (1/18)d_2d_1^3\omega\delta^2h((d_1^2 + 4d_2^2)(\rho_1 \\
&- \rho_2)h + (1/2)\delta\omega^2d_1d_2(d_1\rho_2 + d_2\rho_1))k^5 - (1/3)(d_2(d_1^2 + (1/2)d_2^2)(\rho_1 - \rho_2)h \\
&- (1/12)d_1\delta\omega^2(d_1^3\rho_2 + 3d_1^2d_2\rho_1 + 6d_1d_2^2\rho_2 + 4d_2^3\rho_1))C_g d_1\delta h^3k^4 + 2d_2((d_1^2 + d_2^2)(\rho_1 \\
&- \rho_2)h + (1/2)\delta\omega^2d_1d_2(d_1\rho_2 + d_2\rho_1))d_1\omega\delta h^3k^3(1/3) - C_g(d_1d_2(\rho_1 - \rho_2)h \\
&- (1/3)(d_1^3\rho_2 + 2d_1^2d_2\rho_1 + ((3/2)d_1)d_2^2\rho_2 + (1/2)d_2^3\rho_1)\omega^2\delta)h^5k^2 + 2d_2(d_1(\rho_1 - \rho_2)h \\
&+ (1/3)(d_1^2\rho_1 + ((3/2)d_1)d_2\rho_2 + (1/2)d_2^2\rho_1)\omega^2\delta)\omega h^5k + h^7\omega^2C_g(d_1\rho_2 + d_2\rho_1))/ \\
&(d_2k(h^3\delta^2k^2U_r^2d_2\rho_1((1/6)d_2^2k^2\delta + h^2)\Psi_{10}(\tau)^2 - 2d_2U_r((1/4)d_1^2k^2\delta \\
&+ h^2)k\rho_1((1/6)d_2^2k^2\delta + h^2)\omega\delta h\Psi_{10}(\tau) + h^3\delta^2k^2U_r^2d_1\rho_2((1/6)d_1^2k^2\delta + h^2)\Psi_{20}(\tau)^2 \\
&- 2U_rkd_1\omega((1/4)d_2^2k^2\delta + h^2)\delta((1/6)d_1^2k^2\delta + h^2)h\rho_2\Psi_{20}(\tau) + (1/36)d_1^3d_2^3\delta^2k^6(\rho_1 \\
&- \rho_2) + (1/6)d_2((d_1^2 + d_2^2)(\rho_1 - \rho_2)h + (1/2)\delta\omega^2d_1d_2(d_1\rho_2 + d_2\rho_1))d_1\delta hk^4 + (d_1d_2(\rho_1 \\
&- \rho_2)h + (1/6)\delta\omega^2(d_1^3\rho_2 + 3d_1^2d_2\rho_1 + 3d_1d_2^2\rho_2 + d_2^3\rho_1))h^3k^2 + h^5\omega^2(d_1\rho_2 \\
&+ d_2\rho_1))((1/6)d_2^2k^2\delta + h^2)((1/6)d_1^2k^2\delta + h^2)),
\end{aligned}
\tag{A22}
$$

21 September 2024 04:25:04

Published under an exclusive license by AIP Publishing

$$
\begin{aligned}
M_1(\tau) = {} & (((3d_2(1/2)+d_1)h^4+(1/3)\delta k^2(d_1^3+(3/2(d_1^2))d_2+3/4(d_2^3))h^2+(1/36)\delta^2k^4d_1^2 \\
& \times (d_1^3+3d_2^3))((1/6)d_2^2k^2\delta+h^2)d_2\rho_1\delta^2h^3U_r^2k^2\Psi_{10}(\tau)^2-(2((1/6)d_2^2k^2\delta+h^2))d_2\rho_1((3d_2(1/2) \\
& +d_1)h^6+(1/3)(4(d_1^3+((9/8)(d_1^2))d_2+3/16(d_2^3)))\delta k^2h^4+13\delta^2k^4(d_1^3+(6/13(d_1^2))d_2 \\
& +9/13(d_2^3))d_1^2h^2(1/36)+((1/36)d_1^7+(1/36)d_1^4d_2^3)\delta^3k^6)\delta hU_rk\omega\Psi_{10}(\tau) \\
& -(1/2)(2d_1^2k^2\delta(1/3)+h^2)\delta^2h^3U_r^2((1/6)d_1^2k^2\delta+h^2)^2\rho_2k^2d_1^2\Psi_{20}(\tau)^2+(2d_1^2k^2\delta(1/3) \\
& +h^2)\delta h^3U_r((1/6)d_1^2k^2\delta+h^2)^2\rho_2kd_1^2\omega\Psi_{20}(\tau)-(1/2)\omega^2(d_1^2\rho_2-2d_1d_2\rho_1-3d_2^2\rho_1)h^9 \\
& +k^2d_1^2d_2(\rho_1-\rho_2)h^8-(1/2)(d_1^4\rho_2-((14/3)(d_1^3))d_2\rho_1-5d_1^2d_2^2\rho_1-(1/3)d_1d_2^3\rho_1 \\
& -d_2^4\rho_1)\omega^2k^2\delta h^7+(d_1^2+(1/6)d_2^2)d_1^2k^4(\rho_1-\rho_2)d_2\delta h^6-(1/8)(d_1^6\rho_2-((50/9)(d_1^5))d_2\rho_1 \\
& -(8/3(d_1^4))d_2^2\rho_1-(28/9(d_1^3))d_2^3\rho_1-(20/3(d_1^2))d_2^4\rho_1-(1/3)d_2^6\rho_1)\omega^2k^4\delta^2h^5 \\
& +(1/4)d_1^4(d_1^2+2d_2^2(1/3))k^6(\rho_1-\rho_2)d_2\delta^2h^4-(1/108)d_1^2\omega^2k^6(d_1^6\rho_2-6d_1^5d_2\rho_1 \\
& -(25/2(d_1^3))d_2^3\rho_1-12d_1^2d_2^4\rho_1-((15/2)(d_2^6))\rho_1)\delta^3h^3+(1/54)d_1^6(d_1^2+9d_2^2(1/4))k^8(\rho_1 \\
& -\rho_2)d_2\delta^3h^2+(1/108)d_1^4d_2^3\delta^4k^8\omega^2\rho_1(d_1+d_2)(d_1^2-d_1d_2+d_2^2)h+(1/324)d_1^8d_2^3\delta^4k^{10}(\rho_1 \\
& -\rho_2))(U_r\Psi_{20}(\tau)k\delta-\omega)\delta h^6U_r/((((1/6)d_2^2k^2\delta+h^2)^2d_2^2((1/6)d_1^2k^2\delta \\
& +h^2)^2(h^3\delta^2k^2U_r^2d_1\rho_2(2d_1^2k^2\delta(1/3)+h^2)\Psi_{20}(\tau)^2-(2(2d_1^2k^2\delta(1/3)+h^2))\delta h(d_2^2\delta k^2 \\
& +h^2)U_r\rho_2kd_1\omega\Psi_{20}(\tau)+h^3\delta^2k^2U_r^2d_2\rho_1(2d_2^2k^2\delta(1/3)+h^2)\Psi_{10}(\tau)^2 \\
& -2d_2(2d_2^2k^2\delta(1/3)+h^2)\rho_1\delta hU_r(d_1^2\delta k^2+h^2)k\omega\Psi_{10}(\tau)+h^5\omega^2(d_1\rho_2+d_2\rho_1) \\
& +k^2d_1d_2(\rho_1-\rho_2)h^4+2\delta\omega^2k^2(d_1^3\rho_2+3d_1^2d_2\rho_1+3d_1d_2^2\rho_2+d_2^3\rho_1)h^3(1/3) \\
& +2\delta k^4d_1d_2(d_1^2+d_2^2)(\rho_1-\rho_2)h^2(1/3)+4\delta^2\omega^2k^4d_1^2d_2^2(d_1\rho_2+d_2\rho_1)h(1/3)+4d_1^3d_2^3\delta^2k^6(\rho_1-\rho_2)(1/9))kd_1),
\end{aligned}
\tag{A23}
$$

$$
\begin{aligned}
F_2(\tau) = {} & -h^3U_r(-U_r^2k^2d_1\Psi_{21}(\tau)\delta^2((1/6)d_1^2k^2\delta+h^2)h^3\rho_2\Psi_{20}(\tau)^2 \\
& -2U_rk(\delta h^2\Psi_{11}(\tau)kU_rd_2\rho_1((1/6)d_2^2k^2\delta+h^2)\Psi_{10}(\tau)-(h^2d_1\rho_2((1/6)d_1^2k^2\delta \\
& +h^2)\Psi_{21}(\tau)+d_2((1/4)d_1^2k^2\delta+h^2)\rho_1((1/6)d_2^2k^2\delta+h^2)\Psi_{11}(\tau))\omega)\delta h\Psi_{20}(\tau) \\
& +h^3\delta^2\Psi_{21}(\tau)k^2U_r^2d_2\rho_1((1/6)d_2^2k^2\delta+h^2)\Psi_{10}(\tau)^2+2d_2U_rk\rho_1((1/6)d_2^2k^2\delta \\
& +h^2)\omega\delta h((-(1/4)d_1^2k^2\delta-h^2)\Psi_{21}(\tau)+h^2\Psi_{11}(\tau))\Psi_{10}(\tau)+((1/36)d_1^3d_2^3\delta^2k^6(\rho_1 \\
& -\rho_2)+(1/6)d_2((d_1^2+d_2^2)(\rho_1-\rho_2)h+(1/2)\delta\omega^2d_1d_2^2\rho_1)d_1\delta hk^4+(d_1d_2(\rho_1-\rho_2)h \\
& -(1/6)\delta\omega^2(d_1^3\rho_2-3d_1^2d_2\rho_1-d_2^3\rho_1))h^3k^2-h^5\omega^2(d_1\rho_2-d_2\rho_1))\Psi_{21}(\tau) \\
& -2d_2((1/4)d_1^2k^2\delta+h^2)\rho_1((1/6)d_2^2k^2\delta+h^2)\Psi_{11}(\tau)\omega^2h)\delta/ \\
& (d_2(h^3\delta^2k^2U_r^2d_2\rho_1((1/6)d_2^2k^2\delta+h^2)\Psi_{10}(\tau)^2-2d_2U_r((1/4)d_1^2k^2\delta \\
& +h^2)k\rho_1((1/6)d_2^2k^2\delta+h^2)\omega\delta h\Psi_{10}(\tau)+h^3\delta^2k^2U_r^2d_1\rho_2((1/6)d_1^2k^2\delta+h^2)\Psi_{20}(\tau)^2 \\
& -2U_rkd_1\omega((1/4)d_2^2k^2\delta+h^2)\delta((1/6)d_1^2k^2\delta+h^2)h\rho_2\Psi_{20}(\tau)+(1/36)d_1^3d_2^3\delta^2k^6(\rho_1 \\
& -\rho_2)+(1/6)d_2((d_1^2+d_2^2)(\rho_1-\rho_2)h+(1/2)\delta\omega^2d_1d_2(d_1\rho_2+d_2\rho_1))d_1\delta hk^4 \\
& +(d_1d_2(\rho_1-\rho_2)h+(1/6)\delta\omega^2(d_1^3\rho_2+3d_1^2d_2\rho_1+3d_1d_2^2\rho_2+d_2^3\rho_1))h^3k^2 \\
& +h^5\omega^2(d_1\rho_2+d_2\rho_1))((1/6)d_2^2k^2\delta+h^2)),
\end{aligned}
\tag{A24}
$$

$$
B_1(\tau)=\frac{-\rho_1(U_r\delta\Psi_{10}(\tau)-C_g)}{\rho_1-\rho_2},\quad B_2(\tau)=\frac{\rho_2(U_r\delta\Psi_{20}(\tau)-C_g)}{\rho_1-\rho_2},
\tag{A25}
$$

$$
B_3(\tau)=\frac{1}{\rho_1-\rho_2}\left[\frac{12U_r\delta kh^5(\Psi_{10}(\tau)U_r\delta k-\omega)}{d_1k(d_1^2k^2\delta+6h^2)(2\Psi_{10}(\tau)U_r\delta kh^2-\omega d_1^2k^2\delta-2\omega h^2)}+\frac{12U_r\delta kh^5(\Psi_{20}(\tau)U_r\delta k-\omega)}{d_2k(d_2^2k^2\delta+6h^2)(2\Psi_{20}(\tau)U_r\delta kh^2-\omega d_2^2k^2\delta-2\omega h^2)}\right],
$$

21 September 2024 04:25:04

Published under an exclusive license by AIP Publishing

$$P_1(\tau) = -(-3\delta^2 h^3 U_r^2((1/6)d_1^2k^2\delta + h^2)\rho_2 k^2 d_1((d_1 + 2d_2(1/3))h^4 + (1/6)\delta(d_1^3 + 2d_1d_2^2 + 4/3(d_2^3))k^2h^2 + (1/18)d_2^2\delta^2(d_1^3 + (1/3)d_2^3)k^4)\Psi_{20}(\tau)^2 + 6\delta h U_r((d_1 + 2d_2(1/3))h^6 + (1/6)\delta k^2(d_1^3 + 6d_1d_2^2 + 16/3(d_2^3))h^4 + (1/6)d_2^2\delta^2(d_1^3 + ((2/3)d_1)d_2^2 + (13/9)(d_2^3))k^4h^2 + ((1/54)d_1^3d_2^4 + (1/54)d_2^7)\delta^3k^6)((1/6)d_1^2k^2\delta + h^2)\rho_2 k d_1\omega\Psi_{20}(\tau) + ((1/6)d_2^2k^2\delta + h^2)^2 d_2^2(2d_2^2k^2\delta(1/3) + h^2)\rho_1\delta^2h^3U_r^2k^2\Psi_{10}(\tau)^2 - 2((1/6)d_2^2k^2\delta + h^2)^2d_2^2(2d_2^2k^2\delta(1/3) + h^2)\rho_1\delta h^3U_r k\omega\Psi_{10}(\tau) - 3\omega^2(\rho_2d_1^2 + ((2/3)d_1)d_2\rho_2 - (1/3)d_2^2\rho_1)h^9 - 2k^2d_1d_2^2(\rho_1 - \rho_2)h^8 - \omega^2k^2(d_1^4\rho_2 + (1/3)d_1^3d_2\rho_2 + 5d_1^2d_2^2\rho_2 + ((14/3)d_1)d_2^3\rho_2 - d_2^4\rho_1)\delta h^7 - (1/3)\delta k^4 d_1d_2^2(d_1^2 + 6d_2^2)(\rho_1 - \rho_2)h^6 - (1/12)(d_1^6\rho_2 + 20d_1^4d_2^2\rho_2 + ((28/3)(d_1^3))d_2^3\rho_2 + 8d_2^4d_1^2\rho_2 + ((50/3)d_1)d_2^5\rho_2 - 3d_2^6\rho_1)\omega^2k^4\delta^2h^5 - (1/3)d_1k^6(\rho_1 - \rho_2)(d_1^2 + 3d_2^2(1/2))d_2^4\delta^2h^4 - (1/36)(5(d_1^6\rho_2 + ((8/5)(d_1^4))d_2^2\rho_2 + ((5/3)(d_1^3))d_2^3\rho_2 + ((4/5)d_1)d_2^5\rho_2 - ((2/15)(d_2^6))\rho_1))\omega^2k^6d_2^2\delta^3h^3 - (1/12)d_1k^8(\rho_1 - \rho_2)d_2^6(d_1^2 + 4d_2^2(1/9))\delta^3h^2 - (1/54)d_1^3d_2^4\delta^4k^8\omega^2\rho_2(d_1 + d_2)(d_1^2 - d_1d_2 + d_2^2)h - (1/162)d_1^3d_2^8\delta^4k^{10}(\rho_1 - \rho_2))(U_r\Psi_{10}(\tau)k\delta - \omega)\delta h^6U_r/(2((1/6)d_2^2k^2\delta + h^2)^2d_2((1/6)d_1^2k^2\delta + h^2)^2(h^3\delta^2k^2U_r^2d_1\rho_2(2d_1^2k^2\delta(1/3) + h^2)\Psi_{20}(\tau)^2 - (2(2d_1^2k^2\delta(1/3) + h^2))\delta h(d_2^2\delta k^2 + h^2)U_r\rho_2kd_1\omega\Psi_{20}(\tau) + h^3\delta^2k^2U_r^2d_2\rho_1(2d_2^2k^2\delta(1/3) + h^2)\Psi_{10}(\tau)^2 - 2d_2(2d_2^2k^2\delta(1/3) + h^2)\rho_1\delta hU_r(d_1^2\delta k^2 + h^2)k\omega\Psi_{10}(\tau) + h^5\omega^2(d_1\rho_2 + d_2\rho_1) + k^2d_1d_2(\rho_1 - \rho_2)h^4 + 2\delta\omega^2k^2(d_1^3\rho_2 + 3d_1^2d_2\rho_1 + 3d_1d_2^2\rho_2 + d_2^3\rho_1)h^3(1/3) + 2\delta k^4d_1d_2(d_1^2 + d_2^2)(\rho_1 - \rho_2)h^2(1/3) + 4\delta^2\omega^2k^4d_1^2d_2^2(d_1\rho_2 + d_2\rho_1)h(1/3) + 4d_1^3d_2^3\delta^2k^6(\rho_1 - \rho_2)(1/9))kd_1^2), \tag{A26}$$

$$G_1(\tau) = -3\delta h^4U_r(((1/6)d_2^2k^2\delta + h^2)^2d_2^2(2d_2^2k^2\delta(1/3) + h^2)\rho_1\delta^2((1/3)d_1^2k^2\delta + h^2)h^2U_r^2k^2\Psi_{10}(\tau)^2 - 2((1/6)d_2^2k^2\delta + h^2)^2d_2^2(2d_2^2k^2\delta(1/3) + h^2)\rho_1\delta U_r((1/9)d_1^4\delta^2k^4 + d_1^2\delta h^2k^2 + h^4)k\omega\Psi_{10}(\tau) - (2d_1^2k^2\delta(1/3) + h^2)\delta^2h^2U_r^2((1/6)d_1^2k^2\delta + h^2)^2\rho_2((1/3)d_2^2k^2\delta + h^2)k^2d_1^2\Psi_{20}(\tau)^2 + (2((1/9)d_2^4\delta^2k^4 + d_2^2\delta h^2k^2 + h^4))(2d_1^2k^2\delta(1/3) + h^2)\delta U_r((1/6)d_1^2k^2\delta + h^2)^2\rho_2kd_1^2\omega\Psi_{20}(\tau) - ((1/243)\delta^5d_1^4d_2^4(d_1^4\rho_2 - d_2^4\rho_1)k^10 + 5d_1^2d_2^2h^2(d_1^6\rho_2 + ((9/5)(d_1^4))d_2^2\rho_2 - ((9/5)(d_1^2))d_2^4\rho_1 - d_2^6\rho_1)\delta^4k^8(1/162) + (1/54)(d_1^8\rho_2 + 45d_1^6d_2^2\rho_2(1/2) - 12d_2^4(\rho_1 - \rho_2)d_1^4 - 45d_1^2d_2^6\rho_1(1/2) - d_2^8\rho_1)h^4\delta^3k^6 + (1/4)(d_1^6\rho_2 - (1/9)(8(\rho_1 - 15\rho_2(1/2)))d_2^2d_1^4 - (1/3)(20(\rho_1 - 2\rho_2(1/15)))d_2^4d_1^2 - d_2^6\rho_1)h^6\delta^2k^4 + (d_1^4\rho_2 - 5d_2^2(\rho_1 - \rho_2)d_1^2(1/3) - d_2^4\rho_1)h^8\delta k^2 + h^{10}(d_1^2\rho_2 - d_2^2\rho_1))\omega^2)/(2((1/6)d_2^2k^2\delta + h^2)^2d_2((1/6)d_1^2k^2\delta + h^2)^2(h^3\delta^2k^2U_r^2d_2\rho_1(2d_2^2k^2\delta(1/3) + h^2)\Psi_{10}(\tau)^2 - 2d_2(2d_2^2k^2\delta(1/3) + h^2)\rho_1\delta hU_r(d_1^2\delta k^2 + h^2)k\omega\Psi_{10}(\tau) + h^3\delta^2k^2U_r^2d_1\rho_2(2d_1^2k^2\delta(1/3) + h^2)\Psi_{20}(\tau)^2 - (2(2d_1^2k^2\delta(1/3) + h^2))\delta h(d_2^2\delta k^2 + h^2)U_r\rho_2kd_1\omega\Psi_{20}(\tau) + 4d_1^3d_2^3\delta^2k^6(\rho_1 - \rho_2)(1/9) + 2d_2\delta hd_1(2\delta\omega^2d_1d_2(d_1\rho_2 + d_2\rho_1) + (d_1^2 + d_2^2)(\rho_1 - \rho_2)h)k^4(1/3) + h^3(2\delta\omega^2(d_1^3\rho_2 + 3d_1^2d_2\rho_1 + 3d_1d_2^2\rho_2 + d_2^3\rho_1)(1/3) + d_1d_2(\rho_1 - \rho_2)h)k^2 + h^5\omega^2(d_1\rho_2 + d_2\rho_1))d_1). \tag{A27}$$

Published under an exclusive license by AIP Publishing

21 September 2024 04:25:04

REFERENCES

[1]V. Duchene, "Decoupled and unidirectional asymptotic models for the propagation of internal waves," Math. Models Methods Appl. Sci. **24**, 1–65 (2014).
[2]S. M. Churilov, "Traveling internal waves in a two-layer shallow medium with variable bathymetry and current: Surface and near-bottom flows," Phys. Fluids **35**, 076613 (2023).
[3]M. H. Alford, T. Peacock, J. A. MacKinnon *et al.*, "The formation and fate of internal waves in the South China Sea," Nature **521**, 65–69 (2015).
[4]M. H. Alford, J. A. MacKinnon, H. L. Simmons *et al.*, "Near-inertial internal gravity waves in the ocean," Annu. Rev. Mar. Sci. **8**, 95–123 (2016).
[5]E. C. Reid, T. M. DeCarlo, A. L. Cohen *et al.*, "Internal waves influence the thermal and nutrient environment on a shallow coral reef," Limnol. Oceanogr. **64**, 1949–19655 (2019).
[6]Y. Gong, J. Xie, J. Xu *et al.*, "Spatial asymmetry of nonlinear internal waves in the Lombok Strait," Prog. Oceanogr. **202**, 102759 (2022).
[7]V. W. Ekman, "On dead water," Sci. Results Norw. Polar Exped. **5**, 152 (1904).
[8]A. R. Seadawy, "Fractional solitary wave solutions of the nonlinear higher-order extended KdV equation in a stratified shear flow: Part I," Comput. Math. Appl. **70**, 345–352 (2015).
[9]A. Chabchoub, N. P. Hoffmann, and N. Akhmediev, "Rogue wave observation in a water wave tank," Phys. Rev. Lett. **106**, 204502 (2011).
[10]B. Yang, J. Chen, and J. Yang, "Rogue waves in the generalized derivative nonlinear Schrödinger equations," J. Nonlinear Sci. **30**, 3027–3056 (2020).
[11]R. Li and M. Li, "Generation and evolution of internal solitary waves in a coastal plain estuary," J. Phys. Oceanogr. **54**, 641–652 (2024).
[12]H. Sun, A. Feng, Y. You *et al.*, "Influence of the internal solitary waves on the deep sea mining system," Ocean Eng. **266**, 113047 (2022).
[13]D. J. Benney, "Long non-linear waves in fluid flows," J. Math. Phys. **45**, 52–63 (1966).
[14]C. Yuan, R. Grimshaw, E. Johnson *et al.*, "Generation of nonlinear internal waves by flow over topography: Rotational effects," Phys. Rev. E **101**, 033104 (2020).
[15]M. Stastna and R. Walter, "Transcritical generation of nonlinear internal waves in the presence of background shear flow," Phys. Fluids **26**, 086601 (2014).
[16]C. Yuan, R. Grimshaw, and E. Johnson, "The evolution of second mode internal solitary waves over variable topography," J. Fluid Mech. **836**, 238–259 (2018).
[17]M. Bokaeeyan, A. Ankiewicz, and N. Akhmediev, "Bright and dark rogue internal waves: The Gardner equation approach," Phys. Rev. E **99**, 062224 (2019).
[18]K. Nakayama and K. G. Lamb, "Breather interactions in a three-layer fluid," J. Fluid Mech. **957**, A22 (2023).
[19]J. Sun, X. Tang, and Y. Chen, "Exploring two-dimensional internal waves: A new three-coupled Davey–Stewartson system and physics-informed neural networks with weight assignment methods," Phys. D **459**, 134021 (2024).
[20]M. Stastna and K. G. Lamb, "Large fully nonlinear internal solitary waves: The effect of background current," Phys. Fluids **14**, 2987–2999 (2002).
[21]G. M. Wei, Y. L. Lu, Y. Q. Xie *et al.*, "Lie symmetry analysis and conservation law of variable-coefficient Davey–Stewartson equation," Comput. Math. Appl. **75**, 3420–3430 (2018).
[22]X. Y. Xie and G. Q. Meng, "Dark soliton excitations and collisions for the $(2+1)$-dimensional variable-coefficient Davey–Stewartson-like equations in the plasmas or Bose–Einstein condensates," Chin. J. Phys. **59**, 160–165 (2019).
[23]R. M. El-Shiekh and M. Gaballah, "Solitary wave solutions for the variable-coefficient coupled nonlinear Schrödinger equations and Davey-Stewartson system using modified sine-Gordon equation method," J. Ocean Eng. Sci. **5**, 180–185 (2020).
[24]L. Wang, Y. J. Zhu, F. H. Qi *et al.*, "Modulational instability, higher-order localized wave structures, and nonlinear wave interactions for a nonautonomous Lenells–Fokas equation in inhomogeneous fibers," Chaos **25**, 063111 (2015).
[25]N. Song, R. Liu, M. M. Guo *et al.*, "Nth order generalized Darboux transformation and solitons, breathers and rogue waves in a variable-coefficient coupled nonlinear Schrödinger equation," Nonlinear Dyn. **111**, 19347–19357 (2023).
[26]S. J. Chen, X. Lü, and X. F. Tang, "Novel evolutionary behaviors of the mixed solutions to a generalized Burgers equation with variable coefficients," Commun. Nonlinear Sci. Numer. Simul. **95**, 105628 (2021).
[27]G. Huang, L. Deng, and C. Hang, "Davey–Stewartson description of two-dimensional nonlinear excitations in Bose–Einstein condensates," Phys. Rev. E **72**, 036621 (2005).
[28]H. R. Shaddox, E. E. Brodsky, S. R. Ramp *et al.*, "Seismic detection of oceanic internal gravity waves from subaerial seismometers," AGU Adv. **2**, e2021AV000475 (2021).
[29]J. A. Ródenas and R. Garello, "Internal wave detection and location in SAR images using wavelet transform," IEEE Trans. Geosci. Remote Sens. **36**, 1494–1507 (1998).
[30]S. Wang, Q. Dong, L. Duan *et al.*, "A fast internal wave detection method based on PCANet for ocean monitoring," J. Intell. Syst. **28**, 103–113 (2019).
[31]T. Kataoka, M. Tsutahara, and T. Akuzawa, "Two-dimensional evolution equation of finite-amplitude internal gravity waves in a uniformly stratified fluid," Phys. Rev. Lett. **84**, 1447 (2000).
[32]O. G. Derzho, "Large internal solitary waves on a weak shear," Chaos **32**, 063130 (2022).
[33]J. Xue, H. C. Graber, R. Romeiser *et al.*, "Understanding internal wave–wave interaction patterns observed in satellite images of the Mid-Atlantic Bight," IEEE Trans. Geosci. Remote Sens. **52**, 3211–3219 (2014).
[34]http://www.internalwaveatlas.com/
[35]X. Li, B. Liu, G. Zheng *et al.*, "Deep-learning-based information mining from ocean remote-sensing imagery," Nat. Sci. Rev. **7**, 1584–1605 (2020).
[36]E. S. Selima, Y. Mao, X. Yao *et al.*, "Applicable symbolic computations on dynamics of small-amplitude long waves and Davey–Stewartson equations in finite water depth," Appl. Math. Modell. **57**, 376–390 (2018).
[37]J. Sun, X. Hu, and Y. Zhang, "Quasi-periodic breathers and rogue waves to the focusing Davey-Stewartson equation," Phys. D **460**, 134084 (2024).

21 September 2024 04:25:04

Published under an exclusive license by AIP Publishing